

Assessment of suspended sediment export and dynamics using in-line turbidity sensors and time series statistical models

Andrew M. Tye¹  | Kathryn A. Leeming¹ | Mengyi Gong¹ | Benjamin Marchant¹ | Martin D. Hurst^{1,2}

¹British Geological Survey, Nottingham, UK

²Now at School of Geographical and Earth Sciences, University of Glasgow, University Avenue, Glasgow, UK

Correspondence

Andrew M. Tye, British Geological Survey, Nottingham, NG12 5GG, UK.
Email: atyebgs.ac.uk

Present address

Mengyi Gong, Now at Department of Mathematics and Statistics, Lancaster University, Lancaster, UK.

Funding information

Natural Environment Research Council; BGS National Capability research project, Grant/Award Number: NEE71855

Abstract

The Coln is an ecologically sensitive river in a limestone dominated catchment with no major tributaries. Three in-line turbidity sensors were installed to monitor changes in the dynamics of suspended sediment transport from headwaters to the confluence. The aims were to (i) provide estimates of yield ($\text{t km}^{-2} \text{ year}^{-1}$) and likely drivers of suspended sediment over ~ 3 years and (ii) assess turbidity dynamics during storm events in different parts of the catchment. In addition, the sensor installation allowed a novel wavelet analysis based on identifying groups of turbidity peaks to estimate transport times of suspended sediment through the catchment. Yearly suspended sediment yields calculated for the upper catchment were typically less than $4 \text{ t ha}^{-1} \text{ year}^{-1}$ being similar to other UK limestone or chalk-based rivers. Time series autoregressive integrated moving average models including explanatory variable regression modelling indicated that river discharge, groundwater level and water temperature were all significant predictors of turbidity levels throughout the year. However, high model residuals demonstrate that the models failed to capture random turbidity events. Five parts of the time series data were used to examine sediment dynamics. Plots of scaled discharge versus turbidity demonstrated that in the upper catchment, after initial suspended sediment generation, sediment quickly became limited. In the lower catchment, hysteresis analysis suggested that sediment dilution occurred, due to increasing base flow. The novel wavelet analysis demonstrated that during winter 'sediment events' identified as groups of turbidity peaks, took ~ 18 h to pass from the first sensor in the upper catchment to the second sensor (10.3 km downstream of sensor 1) and 24 h to the third sensor (23.3 km from sensor 1). The work demonstrates the potential for using multiple turbidity sensors and time series statistical techniques in developing greater understanding of suspended sediment dynamics and associated poor water quality in ecologically sensitive rivers.

KEYWORDS

hysteresis, river monitoring, suspended particulate matter, water quality monitoring, wavelet analysis

1 | INTRODUCTION

For many rivers, eutrophication and elevated suspended sediment (SS) concentrations remain potential threats to biodiversity and

aquatic health. Clay, silt and sand sized particles can increase turbidity, thereby reducing light levels; accumulate in fish gills, smother salmonid spawning grounds and benthic habitats; reduce oxygen circulation within the stream bed; and carry sediment sorbed nutrients,

This is an open access article under the terms of the [Creative Commons Attribution](https://creativecommons.org/licenses/by/4.0/) License, which permits use, distribution and reproduction in any medium, provided the original work is properly cited.

© 2024 British Geological Survey (C) UKRI. *Earth Surface Processes and Landforms* published by John Wiley & Sons Ltd.

particularly phosphorus (P), and contaminants through the aquatic environment (Acornley & Sear, 1999; Jarvie et al., 2005; Stutter et al., 2017). Physical impacts of increased fine sediment transport may modify channel geomorphology, increase substrate smothering and create abrasive sediment loads. Currently, no EU Water Framework Directive (WFD) guidelines exist for acceptable quantities of suspended sediment in river waters to achieve 'Good Ecological Status (GES)'. However, a figure of 25 mg L^{-1} suspended sediment (SS) has been suggested for the European Community Freshwater Fish Directive for GES. This figure was used in an assessment of the likelihood of catchments in England and Wales meeting GES standards from agricultural sediment sources (Collins & Anthony, 2008).

Increased concentrations of fine river sediment may occur with land-use change (e.g. timber harvesting; Stott et al., 2001; Stott, 2020) and intensification of land management including that of urban development (Ferreira, Walsh, & Ferreira, 2018). These processes may increase due to climate change with future predictions of UK weather suggesting potential changes in precipitation patterns and intensity (Met Office, 2019). However, whilst the use of buffer strips in agriculture may help reduce eroded soil entering water courses (Boardman et al., 2019; Boardman & Vandaele, 2023), recent studies involving sediment sourcing have demonstrated the importance of bank erosion, and other connective pathways such as farm tracks, roadside erosion, ditches and culverts (Collins et al., 2012; Cooper et al., 2015; Boardman & Vandaele, 2023).

The generation of SS within a catchment depends on the interaction of drivers across different spatial and temporal scales. Sediment is generated from catchment soil and river-bank erosion with factors such as precipitation intensity and duration, erodibility as determined by soil properties (texture, hydrophobicity, crusting), slope (length and steepness) and land cover being important. Additional sources of sediment may result from mass movement events such as landslides, the transfer of sediment via under-field drainage systems, along with human impacts and perturbations within the landscape (Vercruysee, Grabowski, & Rickson, 2017). Catchment hydrological connectivity is important. Fryirs (2013) described connectivity as linkages (longitudinal, lateral and vertical) and blockages (buffers, barriers and blankets). Sediment hysteresis, a process where the relationship between SS and discharge (Q) varies through a storm event, but also is dependent on the previous history of the system further complicates our understanding of SS transport (Haddadchi & Hicks, 2021). Thus, SS can be extremely variable in space and time, determined by the complex system of geomorphological and hydrological processes along with human impacts, interacting over multiple temporal scales (Vercruysee et al., 2020; Vercruysee, Grabowski, & Rickson, 2017). Understanding of SS dynamics within rivers has been increased through sediment sourcing studies (e.g. Collins et al., 2010; Cooper et al., 2015).

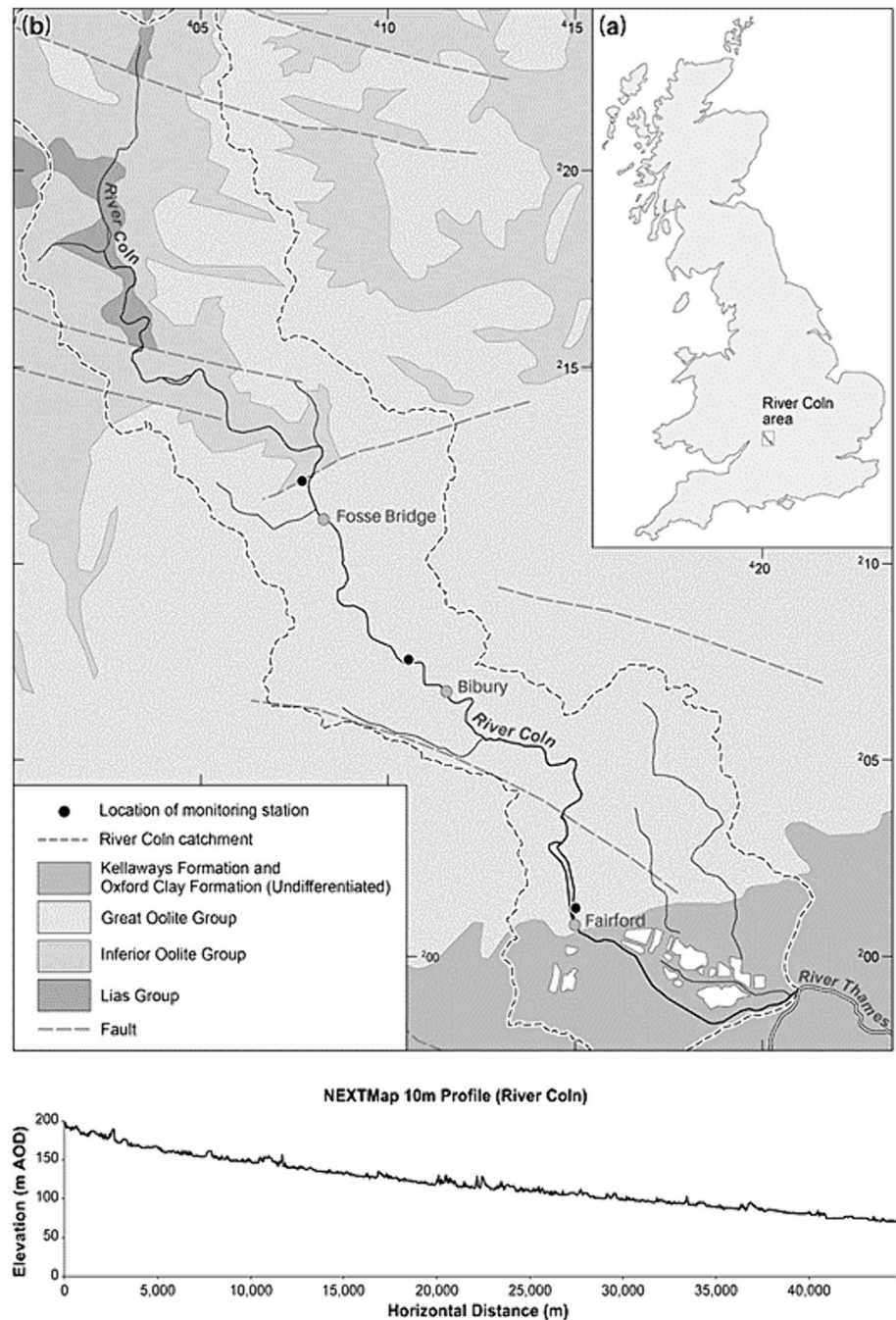
Traditional methods of using SS data along with sample rating curves often underestimate yearly sediment export as they poorly describe large erosion events, hysteresis or have poor curve fitting (Walling, 1977; Asselman, 2000; Malutta et al., 2020). In addition, flux correction methods such as those in Littlewood, Watts, & Custance (1998), which are used when measurements are infrequent can lead to bias (Worrall, Howden, & Burt, 2013). The use of turbidity sensors can improve estimates of SS concentrations and patterns

of transport as they offer high-resolution quasi-continuous measurements through time, which when calibrated, can be considered a proxy for SS (Rasmussen et al., 2009; Stutter et al., 2017). Recognition that other sources of turbidity exist and will be measured is required and may include suspended particles such as phytoplankton, chlorophyll or dissolved organic matter. Recent efforts have tried to characterise these other sources using RGB sensors (Parra et al., 2024). With turbidity sensors, the changing pattern of sediment loads and delivery times can be evaluated to assess water quality and ecosystem response.

Whilst turbidity sensors offer the potential for high resolution measurements, a constraint on their deployment is often cost (Droujko & Molnar, 2022). Typically, they are placed at catchment or sub-catchment outlets so that estimates of upstream SS loss can be made. Thus, opportunities to identify the many physical connections between hydrology, river processes and sediment fluxes in river systems, including catchment processes such as sediment source activation and transport, the influence of land-cover and management, are not fully explored (Droujko & Molnar, 2022). More extensive networks of sensors can develop our understanding of SS transport within catchments and how it may impact ecosystems and physical changes through the length of rivers. These are less often installed. Examples of multi sensor approaches include sensors being placed in catchments in nested designs (e.g. Thollet et al., 2021) or along a river with tributaries entering (Droujko et al., 2023). In addition, Droujko et al. (2023) used a combination of multiple sensors and satellite imagery to assess SS in the Vjosa. However, the use of multiple turbidity sensors sited within a single river without any major tributaries is less common and have the potential to develop a greater understanding of SS dynamics, as no additional inputs of SS entering from tributaries are present. Thus, whilst simpler in focus, they enable study of sediment transport from headwaters to confluence. To the best of our knowledge, this approach to collecting and processing turbidity data has rarely been examined in lowland limestone dominated catchments with high baseflow index (BFI) dominated flow.

Between 2015 and 2018, the British Geological Survey, in collaboration with the National Water Quality Instrumentation Service (NWQIS), part of the Environment Agency (EA), undertook a proof-of-concept study based around turbidity sensors and remote access telemetry. The study was undertaken on the River Coln, a tributary of the River Thames and sited in a limestone dominated catchment (Mackey et al., 1982). Turbidity sensors (combined with sensors for discharge, temperature, pH and conductivity) were placed at three discharge measuring stations along the river from its headwaters to near the confluence with the River Thames. This sensor network produced a unique dataset of high-resolution turbidity and discharge measurements over a 3-year period. The aims of the paper were to (i) calculate sediment yield for upstream catchment areas, (ii) model the principal underlying factors generating turbidity at the three sites, (iii) explore turbidity and discharge relationships and sediment hysteresis, and (iv) identify the distance and travel time of sediment as it passes down the catchment. This last aim reports on a key SS property that typical Q-C analysis cannot provide. It was undertaken using 'wavelet analysis' on groups of identifiable turbidity peaks as they pass by the sensors. This analysis may provide insights into the length of time SS may impair ecological function and how sediment associated pollutants may be transported.

FIGURE 1 Location of (a) the river Coln catchment; (b) the river, catchment geology, and the locations of the monitoring stations at Fosse Bridge, Bibury, and Fairford; and (c) the elevation profile of the river Coln. The map “Contains OS data © Crown copyright and database rights 2023” and the river profile contains ‘NEXTMap Britain elevation data from Intermap Technologies’.



2 | MATERIAL AND METHODS

2.1 | Catchment characteristics

The River Coln is a sub-catchment of the River Thames (Figure 1), with a catchment geology predominantly composed of Oolitic limestone and has a BFI > 0.9 (Bowes et al., 2018). The major soil types within the catchment are part of the Sherborne Soil Association (343d) as mapped by the Soil Survey of England and Wales (Hodge et al., 1984). These are described as shallow well-drained brashy calcareous clayey soils over limestone, associated with slowly permeable calcareous clayey soils. Close to the headwaters is a small area of the Martock Association (711d) which are slowly permeable seasonally waterlogged stoneless silty over clayey and clayey soils over siltstone or shale (Findlay et al., 1984). Maximum altitude in the catchment is 330.2 m above ordnance datum (AOD), and the minimum is 83.5 m

AOD. Three EA gauging stations are positioned within the catchment, at Fosse Bridge, Bibury (NRFA station 39020) and Fairford (NRFA station 39110). Upstream catchment areas for these three stations are 82, 106, and 130 km² respectively. Distance from the river source is approximately 22.2, 32.7 and 45.5 km for Fosse Bridge, Bibury and Fairford respectively, and the altitudes of the three gauging stations are 116.7, 100.6 and 83.7 m AOD. The river rises north of Brockhampton at an altitude of ~200 m AOD, and the greatest fall in altitude is between the headwaters and the Fosse Bridge station (Figure 1). Along the length of the monitored Coln channel, several short spring fed tributaries flow into the river above Fosse Bridge. These are minor and no major tributary exists as a source of SS inputs from other parts of the catchment. Upstream of Bibury, water is diverted into a trout hatchery, which may cause some loss of sediment. There is also bifurcation of the channel between Bibury and Fairford. The catchment is predominantly rural and is dominated by agriculture

(arable and grassland). Aerial photography (APGB high-resolution aerial imagery licensed to BGS from Bluesky International Limited and 'True Orthorectified 25cm National Resolution') shows that within the area of study from Fosse Bridge to Fairford, grassland or buffer strips are present for the length of the river above Fairford, thus decreasing the potential for direct soil erosion input.

2.2 | Monitoring setup

Monitoring equipment at each site was installed in the Spring of 2015 and produced data for ~3 years, to June 2018. Equipment was installed and maintained by the NWQIS, which is part of the EA in England. EXO-Sonde meters, with sensors to measure turbidity, pH, temperature, and conductivity were installed at each monitoring station. Turbidity was measured in formazin nephelometric units (FNU), and sensors were calibrated according to manufacturer's instructions (Exo-user manual). As turbidity measurements may be influenced by mineralogy, particle size and shape of the sediment, specific calibration curves describing the relationship between turbidity and SSC are required for individual rivers or sites (Stutter et al., 2017). To facilitate this, water samplers (ISCO 6712) holding 24 1 L bottles were sited at each monitoring station to collect samples for SS analysis. The ISCO water samplers could be triggered remotely via mobile phone, allowing them to be started prior to expected storm events. This allowed the collection of samples across precipitation events at hourly intervals. The design of the sampling system was based on known characteristics of the Coln obtained from data previously recorded at the monitoring stations. Discussions between NWQIS and the authors were held to obtain the best design for the characteristics of the river which include it being low velocity, shallow and with potentially low flow in dry summers. Water depth at the sampling point at Fosse Bridge was shallow, whilst at Bibury and Fairford, the sampling point was to be positioned before the weirs where flow was measured. A single inlet to the turbidity sensors and water samplers was selected which was placed within ~10 cm of the channel bottom and was considered suitable to allow representative water and sediment samples to be taken. After set-up, equipment was serviced every 3 months according to NWQIS procedures used across their network for the EA. This involved the cleaning of bio-foul from the sensors and their recalibration (EXO User Manual, n.d.).

All sites reported results in real time via telemetry to the NWQIS web site, allowing assessments of measured parameters and enabling data downloads. At the Bibury and Fairford sites, turbidity sensors were placed before weirs at the EA monitoring stations. At Bibury and Fairford, ultrasonic sensing was used to determine water depth. At Fairford, discharge (Q [$\text{m}^3 \text{s}^{-1}$]) was downloaded from the project website set up by NWQIS. At Bibury, water depth data was downloaded from the project website and converted to Q ($\text{m}^3 \text{s}^{-1}$) using the equation for a crimp weir [$Q = 2.28 \times \text{breadth (m)} \times \text{height}^{1.5}$ (m)] where the weir was 9.1 m based on EA guidance (Environment Agency website, n.d.). At Fosse Bridge, a temporary monitoring station was established (Figure 1). Equipment was powered by solar panel-charged batteries. Depth and velocity were calculated using a SonTek-IQ series pressure sensor with in-built velocity beams to profile water velocity in 3-D. Discharge was calculated as $Q = \text{area} \times \text{velocity}$. Hourly Q data was downloaded from the project website.

2.3 | Calibration curve

Table 1 reports information pertaining to the calibration events including precipitation (mm) during the event, the flow and turbidity ranges recorded. Water samples (1 L) collected from the autosamplers were filtered via vacuum using pre-weighed Whatman 0.45 μm cellulose acetate filters to collect SS. Filter papers and collected SS were oven dried at 80°C before weighing. Due to the low amount of sediment collected, no separation of biogenic from mineralogical sediment was undertaken. SS weights were matched to the turbidity reading taken at the same time as the auto-samplers took the sample to form a calibration curve. Samples were collected for calibration curves at the Fosse Bridge and Bibury sites. SSCs were considerably lower and showed little variation at Fairford meaning an individual calibration could not be produced for this site.

2.4 | Data handling and statistical analysis

Data from the turbidity sensors was cleaned prior to analysis, with unexpected spikes within data runs removed. These off-the-scale readings, existing without an obvious reason, were likely caused by vegetation debris being drawn into the measuring system. Some missed measurements occurred in the datasets during sensor maintenance. At Fosse Bridge, measurements started 11 Jun 2015 and finished on the 08 May 2018. A potential total of 25 482 measurements could have been made but there were 1972 missed measurements. Prior to Feb 2018, there were 788 missed measurements for maintenance and when batteries were non-charging, mostly a result of winter snowfall lying on the solar panels. During the period Feb to May 2018, there were 1184 missed measurements, due to extended bad weather and snowfall in the early part of the period ($n = 586$ measurements). However, between April and May 2018, there were only intermittent discharge readings taken leading to a further 598 missed readings. At Bibury, measurements were collected between 22 April 2015 and 04 July 2018, a total of 28 051 readings. There were 118 missed measurements for maintenance during this period. At Fairford, readings started on the 27 April 2015 and finished on the 04 July 2018; a total of 27 519 measurements were made with 428 missed measurements during this period.

Hourly measurements were made at all monitoring stations and at the same time. The guidelines and procedures for computing time series SS and loads from in-stream turbidity sensors of Rasmussen et al. (2011) were followed to convert turbidity readings into monthly and yearly export (t year^{-1}) and yield ($\text{t km}^2 \text{ year}^{-1}$) estimates. Estimates of suspended sediment concentration (SSC) were modelled from turbidity and time associated SSC measurements using linear regression in the R platform (version 4.2.1). Calibration curve estimates of SSC were used in conjunction with river discharge measurements ($\text{m}^3 \text{ s}^{-1}$) to predict SS yields for the hourly measurements. Hourly sediment loads were calculated from Equation (1):

$$SSC_n = \sum_{i=1}^n \frac{(C_i + C_{i-1}) \cdot (Q_1 + Q_{i-1}) \cdot (t_1 - t_{i-1})}{4} \cdot c \quad (1)$$

where SSC_i is the computed SSC, in tons second⁻¹

C_i is the SSC for the i th value in mg L^{-1}

TABLE 1 Information on river properties during calibration storm events.

| Site | Start date | Start time | Precip (mm) | Number of hourly samples | Flow range ($\text{m}^3 \text{s}^{-1}$) | Turbidity range (NFU) |
|--------------|------------|------------|-------------|--------------------------|---|-----------------------|
| Fosse Bridge | 13-08-15 | 0600 | 7.2 | 23 | 0.11–0.21 | 6–29 |
| Fosse Bridge | 19-08-15 | 1300 | 7.6 | 24 | 0.15–0.17 | 7–16 |
| Fosse Bridge | 25-08-15 | 1100 | 1.8 | 23 | 0.12–0.17 | 11–19 |
| Fosse Bridge | 13-12-15 | 1200 | 10.6 | 24 | 0.36–0.67 | 18–67 |
| Fosse Bridge | 27-01-16 | 1600 | 6.6 | 23 | 0.62–0.69 | 17–82 |
| Fosse Bridge | 18-02-16 | 1900 | 8.2 | 23 | 0.86–0.98 | 36–124 |
| Bibury | 13-12-15 | 1200 | 10.6 | 13 | 1.3–1.4 | 1.9–5.3 |
| Bibury | 27-01-16 | 1600 | 6.6 | 23 | 2.7–2.8 | 4.1–7.3 |
| Bibury | 07-02-16 | 0000 | 17.4 | 24 | 3.4–3.6 | 12–19 |

C_{i-1} is the SSC for the i th minus 1 time in mg L^{-1}

Q_i is the stream discharge for the i th value after midnight in $\text{m}^3 \text{s}^{-1}$

Q_{i-1} is the stream discharge for the i th minus 1 value after midnight, in $\text{m}^3 \text{s}^{-1}$

t_i is the time for the i th value after midnight

t_{i-1} is the time for the i th minus 1 value after midnight

c is the constant for converting the units to t day^{-1}

n is the number of instantaneous values within the desired period.

2.5 | Statistical modelling of turbidity in the Coln

Autoregressive integrated moving average models including explanatory variables (ARIMAX) were used to identify the principal underlying factors generating turbidity at the three monitoring sites. Potential variables used in the modelling at each site included the turbidity data (FNU), water velocity (m s^{-1}), discharge ($\text{m}^3 \text{s}^{-1}$), water temperature ($^{\circ}\text{C}$) and conductivity (mS cm^{-1}). There could potentially be a lag or delay between the explanatory factors and the turbidity signal. In addition, due to the high BFI of the catchment, daily groundwater levels were taken from the nearest borehole to the Fosse Bridge site at Coln St Aldwyn. The time series data for each variable were down-sampled from hourly measurements to daily resolution and candidate covariate time series at each location were identified using cross-correlation analyses. These covariates (as described above) were included in the turbidity model according to stepwise selection in a linear model, with residuals modelled with auto-regressive processes. The auto-regressive terms were required to represent temporal correlation in the turbidity time series, which if ignored, could potentially lead to the significance of the explanatory factors being exaggerated. An ARIMAX model was fitted for turbidity at each location according to these steps using the ‘arimax’ package in the R platform.

2.6 | Statistical modelling of substantial turbidity events

Understanding the dynamics of SS transport down the river channel, from headwaters to confluence, during precipitation, events is important to understanding the negative impacts on water quality that SS can cause. Wavelet analysis was undertaken to estimate the travel

time of identifiable ‘clusters of SS peaks’ through the river system using the three in-line turbidity sensors. The wavelet approach contrasts and adds additional information to traditional sediment v discharge plots. These provide information relating to peak SS concentrations at monitoring stations during storm events. Three sections of hourly turbidity time series were examined these being (i) Dec 2015 to Feb 2016, (ii) Jan–Feb 2017, and (iii) July–Sept 2017. These events cover two periods of winter precipitation when turbidity was high and one summer period when turbidity was low. The non-decimated wavelet transform (Nason & Silverman, 1995) was used to compare the information at different temporal scales within the turbidity signals. This allows for comparison of changes in the turbidity values over different time scales across the three locations. The non-decimated wavelet transform generates information about the time series at each time point over multiple temporal scales or frequencies. This transform generates a wavelet coefficient for each scale j and time step t : $d_{j,t} = \sum_k \varphi_{j,k} Y_{t-k}$, where φ represents a discrete wavelet, Y is the time series of length T , and the timescale ranges from 0 (coarsest) to $\lfloor \log_2(T) \rfloor - 1$ (finest), and k is the index of the sum used to apply the discrete wavelet over time. The scales correspond to time periods of power of two length. The wavelet coefficients from the scale with wavelength 128 h were used to assess the long duration peaks. This was the closest scale to the duration of interest and allowed comparison of the relative timing of these peaks by applying the cross-correlation function to the wavelet coefficients from the different locations on the river. High values in the cross-correlation results suggest time lags with similar long duration peaks. Wavelets were also used as a smoothing method for the time series. The forwards decimated wavelet transform was performed; then, the three finest scales of coefficients (corresponding to wavelengths 8 h or shorter) removed before back transformation of the series. This provides a smooth representation of the signal by removing high-frequency perturbations. Wavelet computations were performed using the ‘wavethresh’ package in R (Nason, 2016).

Thus, the wavelet coefficients contain information relating to the shape of the signal at different temporal scales. By comparing the cross-correlation at different lags at the sites, the time separations that show the greatest similarity in the shape of the peak can be identified. High correlation between the coefficients would indicate that the peaks are of similar shapes, and the corresponding time delay of the peak between gauges can be quantified. Smoothing the series using the wavelet transform allows for high-frequency fluctuations to be removed without dampening the peaks.

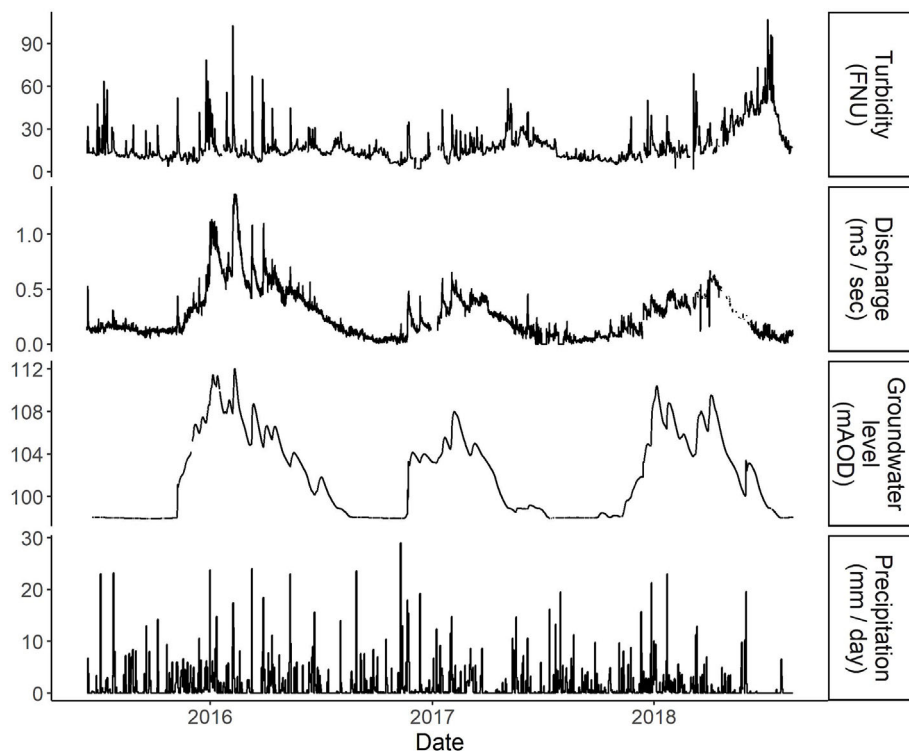


FIGURE 2 Recorded turbidity, discharge, groundwater level, and precipitation for the Fosse bridge monitoring station. [Color figure can be viewed at [wileyonlinelibrary.com](https://onlinelibrary.wiley.com/doi/10.1002/esp.5952)]

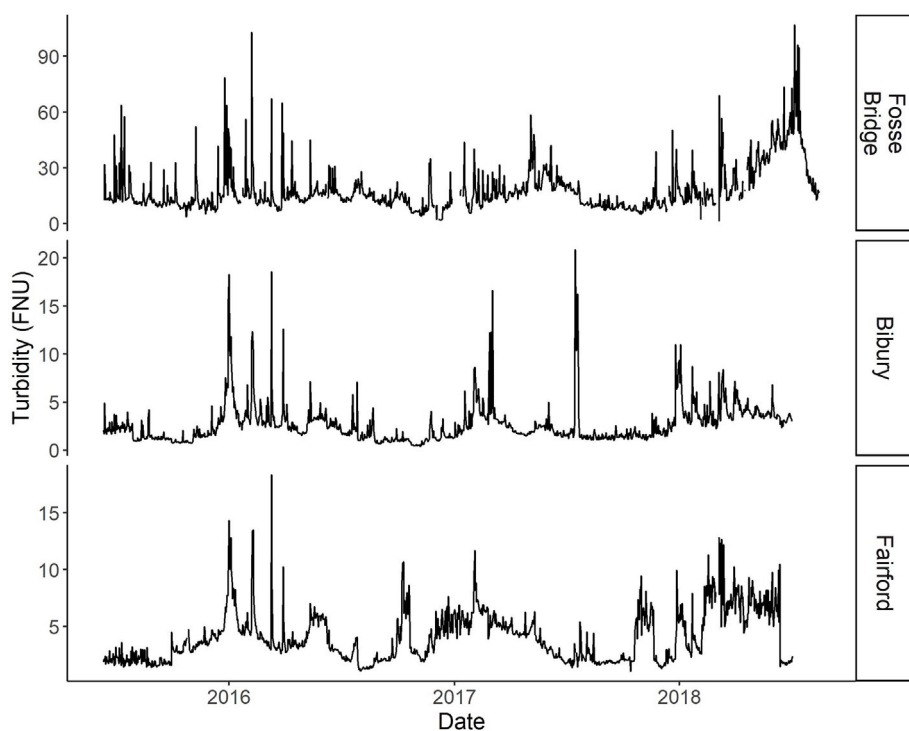


FIGURE 3 Turbidity (FNU) measurements at the three monitoring sites (note differing y-scale). Data is down-sampled data to a daily mean to provide a smoother representation of data. Please note that the sampling period at Fosse bridge extended beyond the other sites. FNU, formazin nephelometric units. [Color figure can be viewed at [wileyonlinelibrary.com](https://onlinelibrary.wiley.com/doi/10.1002/esp.5952)]

3 | RESULTS

3.1 | Seasonal patterns of precipitation, groundwater elevation and river discharge

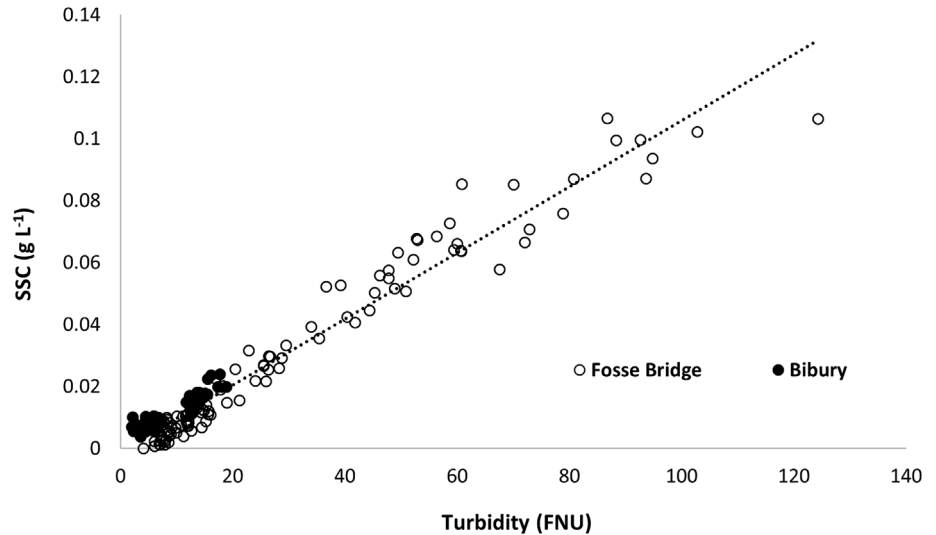
Figure 2 reports general changes in the annual responses of turbidity, discharge, groundwater level and precipitation at Fosse Bridge. Similar plots for the Bibury and Fairford monitoring stations can be found in SI:1. Groundwater rises rapidly in late autumn when evapotranspiration decreases and recharge dominates, with highest levels being found in late winter before groundwater and discharge rates decline

in late spring and summer. Similar responses were found for the Bibury and Fairford sites. Figure 3 shows the turbidity patterns for each of the three monitoring stations over the measurement period. Results show a general decrease in turbidity (FNU), and thus SSC from Fosse Bridge down to Fairford.

3.2 | Calibration curve

Whilst identical EXO-Sonde turbidity sensors were used at each site and were similarly maintained, calibration curves assessing the

FIGURE 4 Relationship between turbidity (FNU) and suspended sediment (g L^{-1}) for the Fosse bridge and Bibury monitoring sites. FNU, formazin nephelometric units.



relationship between turbidity and SS were produced for both the Fosse Bridge and Bibury sites. Figure 4 shows the relationship between turbidity and SSC (g L^{-1}) for the Fosse Bridge and Bibury sites. Both individual site calibration curves were highly significant ($P < 0.01$). The calibration curve for Fosse Bridge was $y = 0.0011x - 0.0013$ (Table 2), whilst for Bibury, it was $y = 0.0014x + 0.0031$ (Table 3) where x is turbidity (FNU) and y is SSC (g L^{-1}). At Fairford, SS had very low variation in concentrations through the storm events. Thus, a suitable calibration curve could not be produced. Therefore, no estimates of export and yield were made at Fairford based on a specific calibration.

3.3 | Catchment SS export and yields

Using the calibration curve relating turbidity to SSC monthly, yearly sediment export (t) and yield ($\text{t km}^{-2} \text{ year}^{-1}$) were estimated. Yearly export (the annual sum of $Q * \text{SSC}$) and yield ($Q * \text{SSC} / \text{upstream catchment area} [\text{km}^2]$) estimates for the monitoring stations at Fosse Bridge and Bibury are presented in Table 4. Results suggest that, in terms of export (t), the estimated SS export found at Bibury was only slightly greater than that estimated at the Fosse Bridge monitoring station. Figure 5 shows the relationship between estimated monthly SS export and monthly river discharge at the Fosse Bridge and Bibury monitoring stations. The relationship between discharge and SS export showed a greater export occurring at lower discharge rates at Fosse Bridge than at Bibury, possibly reflecting the slightly greater slope in the upper catchment. Typically for the Fosse Bridge and Bibury monitoring stations, sediment yield was $< 4 \text{ t km}^{-2} \text{ year}^{-1}$ based on their respective upstream catchment areas. Figure 6 shows estimated monthly yields (t km^2 per month) from the Fosse Bridge site using its upstream contributing area. Similar figures are shown in SI:2 for the Bibury site. Both sites followed similar patterns. Highest yields were found in January and February 2016, coinciding with winter precipitation, high groundwater and saturated soils. At Fosse Bridge, sediment yields for these months were greatest with highest yields being $\sim 0.5 \text{ t km}^{-2}$ per month. Figure 7(a) shows a comparison of the monthly exports calculated at the Fosse Bridge and Bibury monitoring stations. Generally, an increase in export was found at the lower

TABLE 2 Summary of calibration model for Fosse bridge where turbidity (FNU) is converted to estimates of suspended sediment concentration.

Number of measurements: 141
Model: $\text{SSC} (\text{g L}^{-1}) = 0.0001052 * \text{turbidity} - 0.001269$

Coefficients

| | Estimate | Std. error | t-value | Pr(> t) |
|-----------|---------------------|--------------------|---------|----------------------|
| Intercept | $-1.269\text{e}-03$ | $8.150\text{e}-04$ | -1.557 | 0.122 |
| Turbidity | $1.052\text{e}-03$ | $1.949\text{e}-05$ | 53.973 | $< 2\text{e}-16$ *** |

Residual standard error: 0.006228 on 140 degrees of freedom. Adjusted R -squared: 0.9538. F -statistic: 2913 on 1 and 140 DF. p -value: $< 2.2\text{e}-16$. RMSE = 0.00622.

Abbreviations: FNU, formazin nephelometric units; SSC, suspended sediment concentration.

station. However, in some months, the export at Bibury was smaller than at Fosse Bridge, indicating that some storage of sediment was occurring in the river between the monitoring stations. This occurred in May 2016, October 2016 and April 2017. The difference in sediment export in these months was $< 4 \text{ t}$. In Figure 7(b), the relationship between the difference in export between Fosse Bridge and Bibury is plotted against groundwater head level at Coln St Alydwyn. There is a positive relationship ($R^2 = 0.71$) between the groundwater head level (m) and the difference in the sediment budget between the two sites.

3.4 | Results of modelling turbidity

ARIMAX models were used to determine factors responsible for driving increases in turbidity in relation to external variables. Final model selection provides information on the hydrological variables that contribute towards turbidity levels. All of the potential predictor variables were included in the Fosse Bridge fitted model which was of the form

$$Y_t = \beta_0 + \beta_1 \Delta W_t + \beta_2 \Delta W_{t-1} + \beta_3 \Delta W_{t-2} + \beta_4 \Delta W_{t-3} + \beta_5 G_t + \beta_6 T_t + X_t$$

where Y_t is turbidity (FNU), W is the time series of water discharge, G is the time series of groundwater level, T is the temperature, Δ

TABLE 3 Summary of calibration model for Bibury bridge where turbidity (FNU) is converted to estimates of suspended sediment concentration.

| Number of measurements: 58 | | | | |
|---|-----------|------------|---------|--------------|
| Model: $SSC (g L^{-1}) = 0.000975 * turbidity + 0.003091$ | | | | |
| Coefficients | | | | |
| | Estimate | Std. error | t-value | Pr(> t) |
| Intercept | 3.091e-03 | 4.987e-04 | 6.199 | 7.19e-08 *** |
| Turbidity | 9.758e-04 | 5.126e-05 | 19.037 | < 2e-16 *** |

Residual standard error: 0.001916 on 56 degrees of freedom. Adjusted R-squared: 0.8638. F-statistic: 362.4 on 1 and 56 DF. p-value: < 2.2e-16. RMSE = 0.001916.

Abbreviations: FNU, formazin nephelometric units; SSC, suspended sediment concentration.

TABLE 4 Yearly total exports (t year⁻¹) and calculations of sediment yield (t km² year⁻¹).

| Monitoring site | Upstream catchment area (km ²) | Distance from source (km) | Sediment export (t year ⁻¹) | | | | Sediment yield (t km ² year ⁻¹) | | | |
|-----------------|--|---------------------------|---|-------|-------|--------|--|------|------|--------|
| | | | 2015* | 2016 | 2017 | 2018** | 2015* | 2016 | 2017 | 2018** |
| Fosse Bridge | 82 | 22.6 | 54.2 | 200.0 | 100.2 | 45.7 | 0.66 | 2.43 | 1.22 | 0.56 |
| Bibury | 106 | 32.7 | 87.2 | 398.8 | 181.2 | 250.5 | 0.83 | 3.76 | 1.71 | 2.36 |

*2015 calculated over period Mar–Dec.

**2018 calculated over period Jan to June.

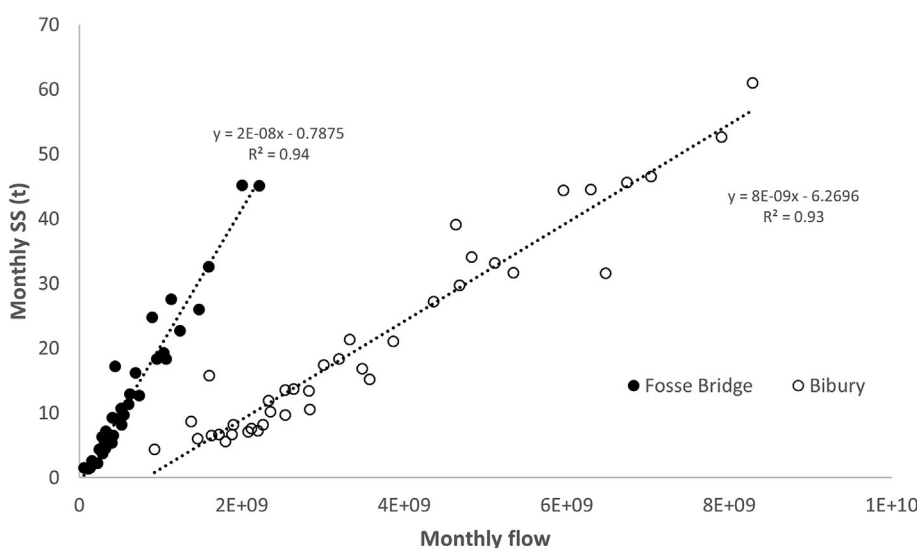


FIGURE 5 Relationship between monthly discharge (L) and suspended sediment export (t).

represents the difference operator and the temporally correlated residuals, X_t , are represented by an AR(3) process, an autoregressive process of the form $X_t = \alpha_1 X_{t-1} + \alpha_2 X_{t-2} + \alpha_3 X_{t-3} + \epsilon_t$. The α and β coefficients are used to minimise the model errors, ϵ .

The Bibury series had fitted model

$$Y_t = \beta_0 + \beta_1 \Delta W_t + \beta_2 \Delta W_{t-1} + \beta_3 \Delta W_{t-2} + \beta_4 \Delta W_{t-3} + \beta_5 G_t + \beta_6 T_t + X_t$$

At Fairford, the fitted model was

$$Y_t = \beta_0 + \beta_1 \Delta W_t + \beta_2 \Delta W_{t-1} + \beta_3 G_t + \beta_4 T_t + X_t$$

where X is an AR(3) process.

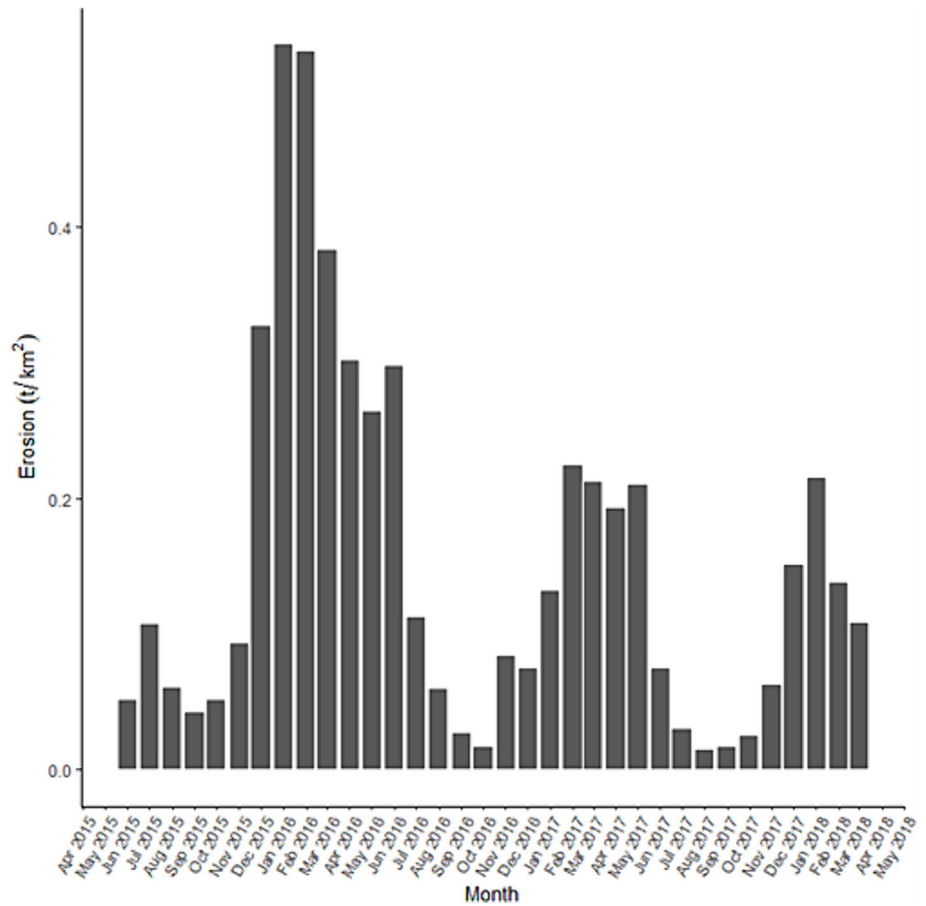
In all models, the water discharge series was included as a differenced series due to high correlation with the groundwater series indicating that increases in turbidity occur as groundwater levels rise. Figure 8 shows the model outputs of turbidity against the sensor

turbidity data. At all three sites, the modelled data follows the pattern of observed data, but random high turbidity events are often not captured effectively. The closeness of the model to the long-term turbidity trends is in part due to the autoregressive error process. Removing these temporally correlated terms increases the RMSE by at least 28% in all three locations.

3.5 | Sediment-turbidity plots and hysteresis

Traditionally, SS dynamics in rivers have been examined by combining information on turbidity or SSC, discharge and time. Turbidity and discharge plots enable the response of turbidity against discharge over time at sampling locations, whilst hysteresis plots integrate turbidity and discharge to provide information regarding sediment availability and transport in relation to discharge and time. Using several monitoring stations down a river enables a comparison of response at

FIGURE 6 Estimated monthly sediment yields ($t\ km^{-2}$) at the Fosse bridge monitoring site. [Color figure can be viewed at wileyonlinelibrary.com]



different locations. Figures 9–13 show a selection of plots of normalised discharge and sediment at the monitoring stations and their accompanying hysteresis plots. These cover events during the periods selected for analysis (Dec 2015 to Jan 2016 and Jan–Feb 2017). Prior to plotting, data was smoothed over a period of 6 h to remove high frequency fluctuations that obscure the discharge and hysteresis curves. SSC patterns were examined for the following time periods:

1. 30th Dec 2015 to 3rd Jan 2016

Total precipitation for this storm period was 33 mm, with 23.8 mm of rain falling on the 31st December. For all three monitoring stations, the turbidity peak occurred before the water discharge peak suggesting that base flow continued to increase river discharge, after the turbidity peak generated by the rainfall event has passed (Figure 9). For Fosse Bridge, where the turbidity peak occurred at 4 am Dec 31st, and Bibury, where the turbidity peak occurred at 12 pm Dec 31st, a rapid decline in turbidity occurred after peak SS. At Fairford, a double peak occurred. The first occurred at 6 am 30th Dec shortly after the onset of the precipitation event, and the second turbidity peak occurred at 3 am Dec 31st, coinciding or coming shortly before the turbidity peaks at Fosse Bridge and Bibury. The hysteresis plots show different patterns at the three sites over the time period. At Fosse Bridge, there is clockwise hysteresis suggesting that sediment availability is declining as discharge increases. There is a rapid drop off in turbidity as the event progresses and discharge is high suggesting a limitation on sediment availability. At Bibury, a similar initial response is found to that at Fosse Bridge, where a clockwise

hysteresis pattern is initially observed. However, low sediment supply and dilution of the sediment result in a rapid drop off at high discharge rates. At Fairford, the turbidity hysteresis response pattern is similar to that of the raw data, as discharge increases almost linearly. The pattern of response again suggests that the supply of sediment is limited and is diluted with increasing discharge resulting in peaks and sudden drops in turbidity at higher discharges.

2. 27th–30th Jan 2016

Precipitation for this period was 12.4 mm, with 5.4 and 5.8 mm of rain falling on the 27th and 30th January, respectively. At Fosse Bridge (Figure 10), the turbidity and discharge peaks occur almost at the same time (~ 8 pm on the Jan 27th) producing an almost linear response in the hysteresis pattern. At Bibury, two sediment peaks occur. A small peak occurs ~ 2 pm on 27th Jan that coincides with peak discharge (local initial resuspension), and a second higher concentration peak is found at ~ 10 am on 28th Jan, which occurs after peak discharge, which suggests that SS has been transported from higher up in the catchment. At Fairford, the turbidity peak which is recorded ~ 11 am on 28th Jan occurs after peak discharge thus producing anti-clockwise hysteresis graphs. Anti-clockwise hysteresis may occur when storm discharge peaks pass through the catchment before the sediment peak.

3. 30th Jan to 1st February 2016

Precipitation for this period was 6 mm, with 5.8 mm falling on 30th January. At Fosse Bridge, the turbidity peak recorded at ~ 11 am

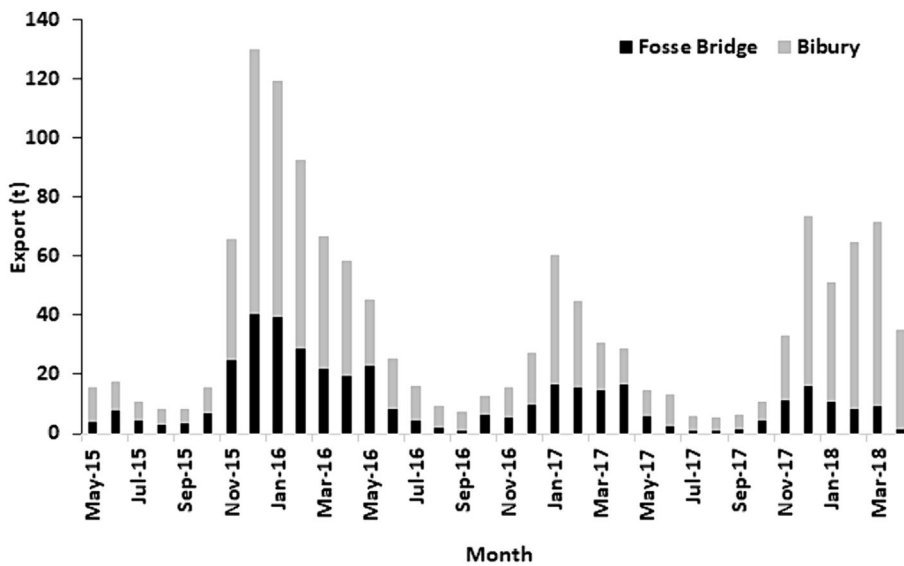
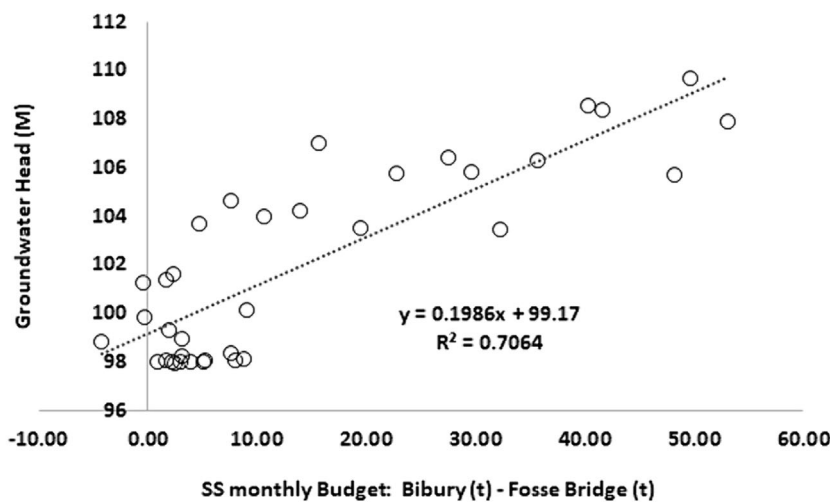


FIGURE 7 In (a), the comparison of monthly sediment yields (t km^2) at Fosse bridge and Bibury sites showing those months when the river between the two sites acted as a sediment sink. This occurs when there is less export (t) at Bibury than at Fosse bridge. In (b), the relationship in the difference of sediment transported between the two sites and mean monthly groundwater head at Coln St Aldwyn borehole is shown.



on 30th January is slightly in front of the storm discharge peak (Figure 11). This may be due to a pulse of fine sediment being produced before the flood stage arrives. However, the overall clockwise hysteresis suggests that sediment availability is limited. At Bibury, a double SS peak is recorded at 8 am on 30th Jan and the second at ~9 pm on 30th Jan. In both cases, the turbidity and discharge peaks occur almost simultaneously, although the second turbidity peak is higher. This produces tight anticlockwise hysteresis plots. Again, the double sediment peak suggests an initial resuspension of sediment followed by later transport of sediment from upstream. At Fairford, the turbidity peak occurs very slightly in front of the discharge peak but this quickly declines whilst discharge remains high. This can be seen in the hysteresis plot where there is an initial clockwise direction before a rapid decrease in sediment availability at high discharges.

4. 15th–20th Jan 2017

Precipitation for this storm period was 13.1 mm, with 4.2, 4.8 and 3.9 mm falling on 15th, 16th, and 17th January respectively. At Fosse Bridge (Figure 12), the turbidity and the discharge peak occurred

almost at the same time (~10 pm Jan 16th) and a relatively tight clockwise hysteresis graph is produced suggesting an almost linear response but with sediment becoming increasingly unavailable. At Bibury, there appears to be an initial linear type relationship between turbidity and discharge. The turbidity peak occurs ~10 pm on 17th Jan, but rapid exhaustion of sediment supply occurs before peak discharge leading to a large drop in turbidity measurements which may reflect sediment dilution. At Fairford, several sediment peaks are found with the highest occurring ~1 pm on 18th Jan. However, no overall hysteresis pattern is obtained for a long event with multiple peaks.

5. 1st–5th Feb 2017

Precipitation for this storm period was 24.8 mm, with the majority (14.8 mm) falling on 1st February, and the remainder spread through the period. At Fosse Bridge (Figure 13), the peaks of turbidity and discharge occur together, peaking ~3 pm on 1st February. Turbidity drops off quickly suggesting a limitation to sediment supply and demonstrated by the clockwise hysteresis plot. At Bibury, the turbidity

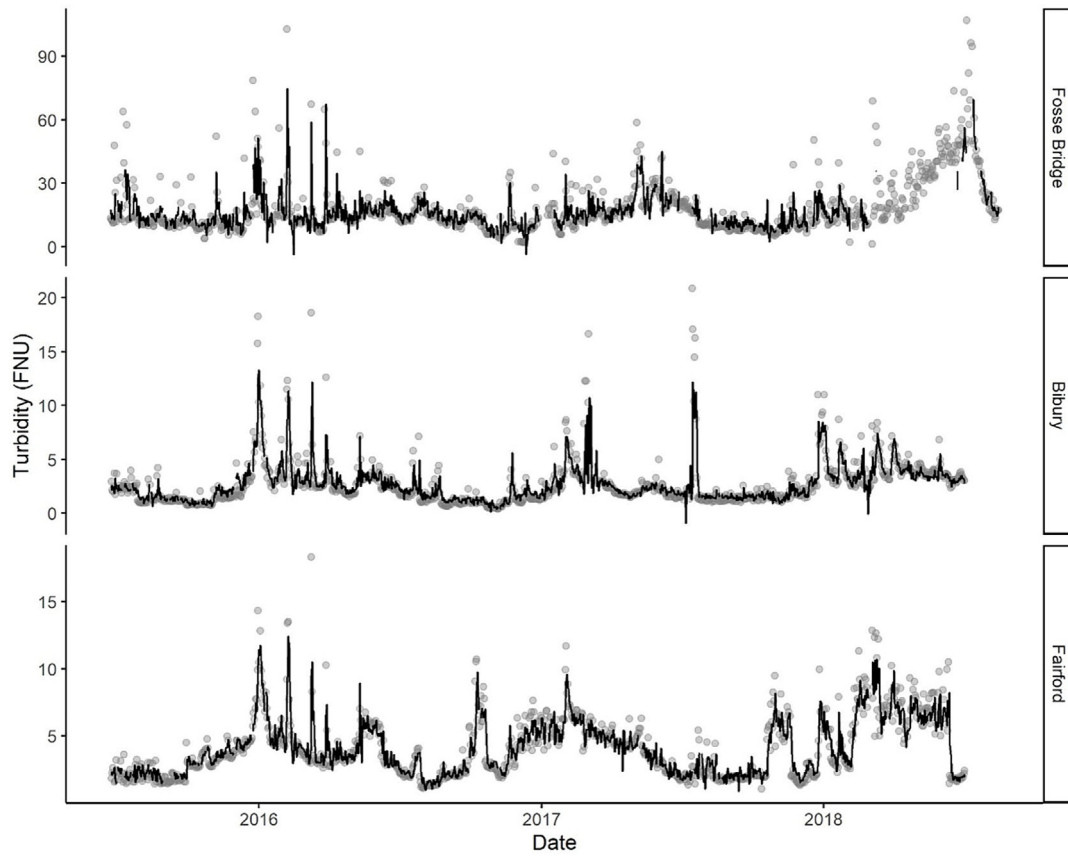
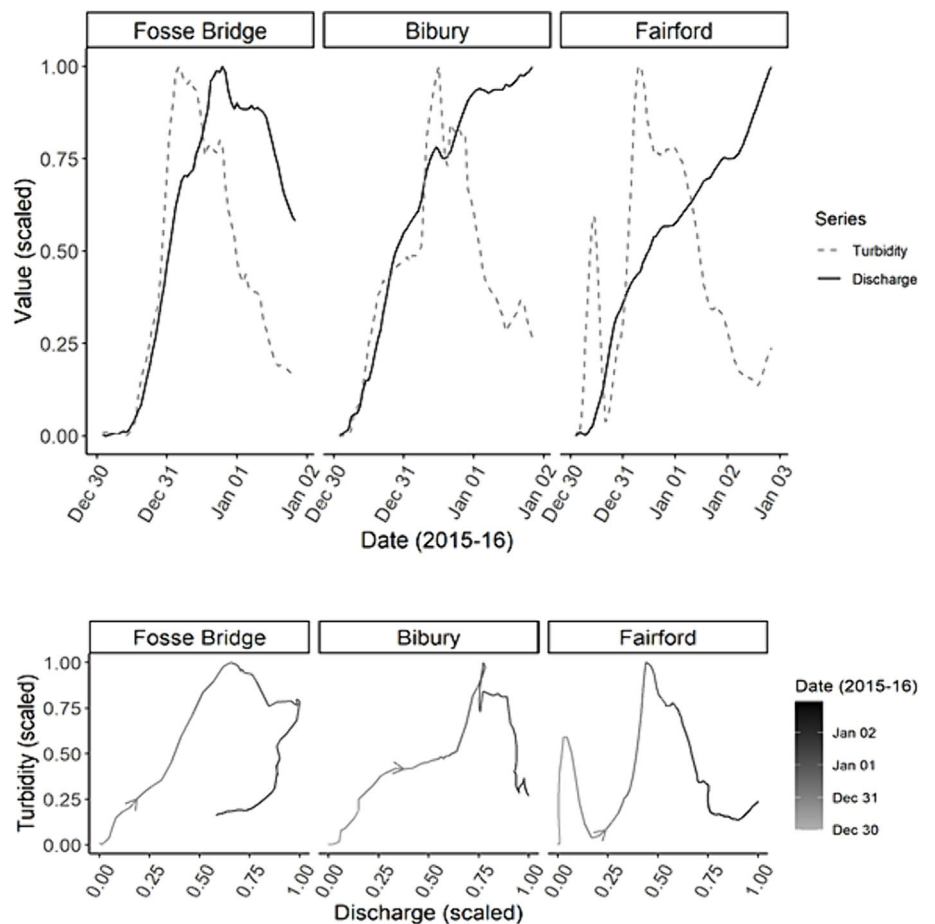


FIGURE 8 Turbidity measurements (grey circles) and the ARIMAX model fit (black line). ARIMAX, autoregressive integrated moving average models including explanatory variables. [Color figure can be viewed at wileyonlinelibrary.com]

FIGURE 9 Diagram showing scaled (a) discharge and turbidity plots and (b) hysteresis plots for period 30th Dec 2015 to 3rd January 2016. [Color figure can be viewed at wileyonlinelibrary.com]



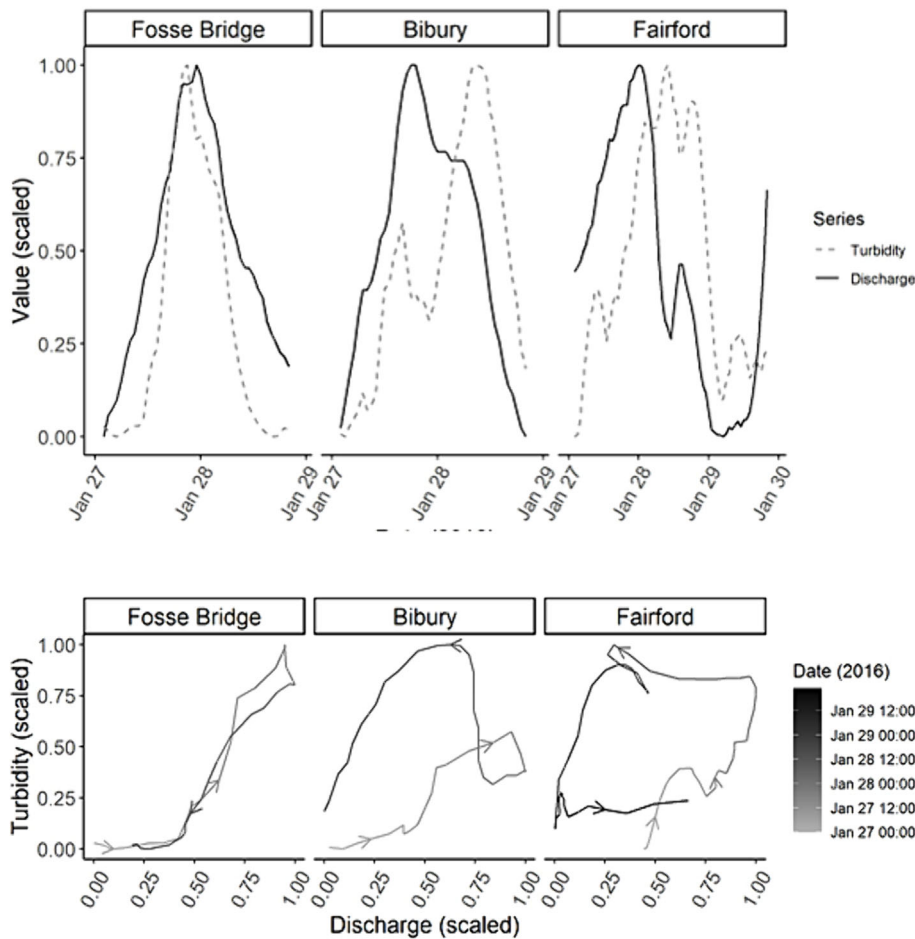


FIGURE 10 Diagram showing scaled (a) discharge and turbidity plots and (b) hysteresis plots for period 27th–30th January 2016. [Color figure can be viewed at wileyonlinelibrary.com]

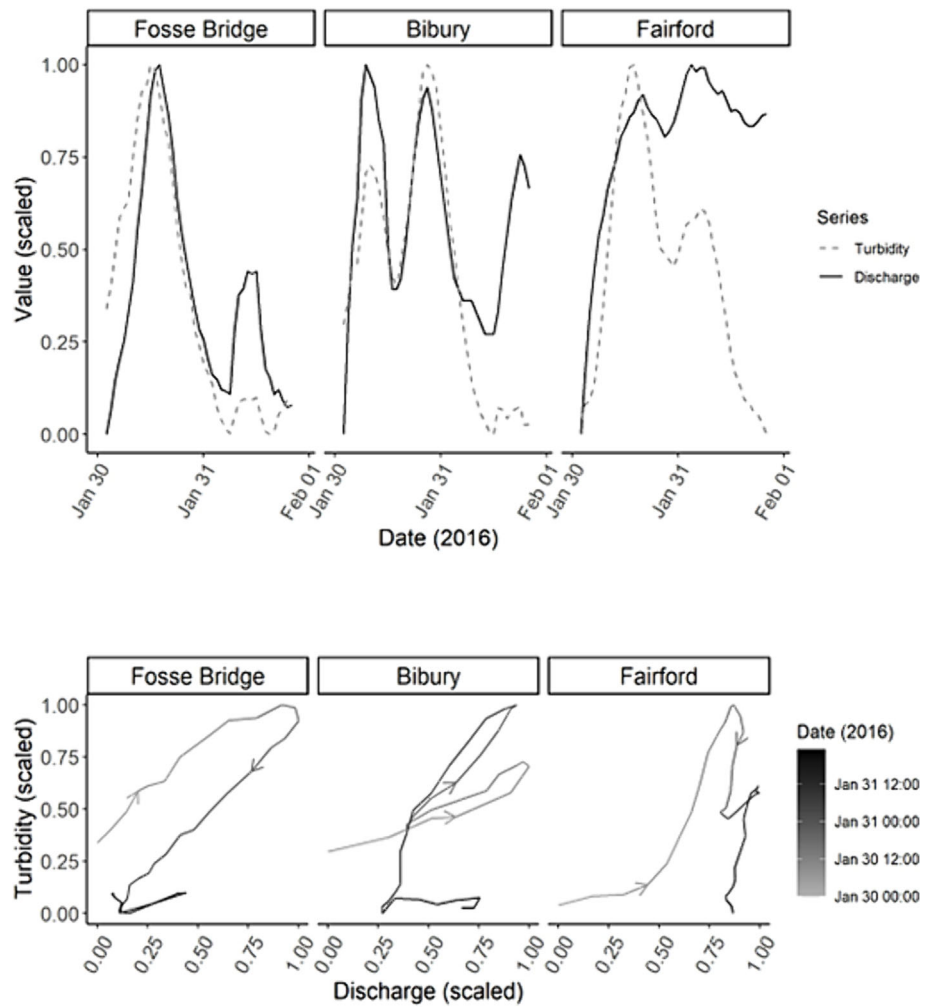
peak occurs ~ 7 am on 2nd Feb, whilst there is a continual increase in discharge afterwards. The hysteresis plot suggests some initial SS availability, but the very tight anti-clockwise loop suggests a sudden drop off in sediment availability. At Fairford, the turbidity response is similar to that at Bibury, showing a rapid drop in turbidity after ~ 2 pm on 2nd Feb as discharge increases.

3.6 | Wavelet modelling significant turbidity events

When using several turbidity monitoring stations along a river, it is possible to determine times of peak SS concentrations at each site using turbidity (SSG) versus discharge (Q) plots (Figures 9–13). The descriptions in Section 3.6 demonstrate the complexity of SSC over time, where several peaks often occur during events that last several days. These peaks related to initial resuspension, along with the downward movement of SS from the upper catchment. They may also be influenced by factors local to the individual monitoring stations, such as the rainfall pattern across the catchment. In contrast, wavelet analysis (Section 2.6) can provide estimates of how quickly SS is moving through the river system, by tracking identifiable turbidity peak groups, whilst the smaller, more transient and random events are smoothed out. Thus, the wavelet analysis aims to identify similar patterns of turbidity response from a series of peaks, which are separated by time lags, giving an approximation of the travel time and possible distance of travel of SS down the river system.

Wavelet analysis was undertaken for three sections of the turbidity time series. These include the two periods of data examined in Section 3.6 (Dec 2015 to Feb 2016 and Jan–Feb 2017) and a summer period (July–Sept 2017). The first example studied was the period between Jan and Feb 2017. The turbidity time series plots for the periods can be found in Figure 14(a). After applying the wavelet transforms, the wavelet coefficients can be seen in Figure 14(b) as a series of pyramid-like shapes present in the plots for each location. The wavelet coefficients represent how much variation there is in the signal at each scale (analogous to frequency, in scales corresponding to time lengths in powers of 2). The pyramid-like shapes correspond to the peaks and sharp spikes in the turbidity data. In particular, the pyramid shapes (outlined with black triangles) for each of the two time periods appear to move towards the right going down the subplots (i.e. from Fosse Bridge to Fairford), indicating that the peaks originating at Fosse Bridge can be located later in the time series data further down the catchment. In Figure 14(c), the estimated cross-correlation functions are shown for the different locations at scale 2, which corresponds to changes occurring over a period of around 128 h. Peaks in the negative lag parts (x -axis) of the plots indicate that the first named location is being led by the second named location; for example, in the 'Bibury and Fosse' plot, the Bibury coefficients are lagging behind the Fosse Bridge coefficients by around 16–18 h, identified by the time lag with the highest values of estimated auto-correlation functions (ACF). Similarly, the Fairford series appears to lag the Fosse Bridge series by around 19–25 h, but the Fairford and Bibury plots do not show a clear lead–lag relationship between these locations. The

FIGURE 11 Diagram showing (scaled) (a) discharge and turbidity plots and (b) hysteresis plots for period 30th January to 01 February 2016. [Color figure can be viewed at wileyonlinelibrary.com]



delays found by analysing the cross-correlation plots are demonstrated in Figure 14(d), where the wavelet smoothed versions of each series are plotted, with the Fosse Bridge series delayed by 18 h (Figure 14(d)) and 23 h (Figure 14(e)). The shifted Fosse Bridge series shows a similar pattern to the Bibury series (left); however, the relationship between Fosse Bridge and Fairford (right) is not as clearly aligned, with the peaks being potentially closer together in the Fairford series. This example suggests that a cluster of identifiable turbidity peaks is generated in the upper catchment prior to Fosse Bridge, which can then be seen strongly at Bibury (10.1 km downstream) and with a weaker signal at Fairford (22.9 km downstream). Reduction in turbidity FNU would suggest that the initial turbidity peak is being diluted, although the increase in turbidity between Bibury and Fairford may suggest that a small amount of additional resuspension or bank erosion has occurred.

A graphical analysis was undertaken for the period December 2015 to February 2016. The same number of hours delay as recorded for the peak clusters for the Jan–Feb 2017 (18 h Fosse Bridge to Bibury and 23 h for Fosse Bridge to Fairford) were applied to obtain the time-shifted line (the lower graph in each case) in Figure 15. The peaks of these shifted lines appear to be slightly later than the SS patterns recorded at Bibury (a) and Fairford (b). As the shifted Fosse Bridge line has peaks slightly after those in the upper plots, the delays between the peaks at different locations are present but are slightly shorter than in the Jan–Feb 2017 segment. The final example is that of a summer period occurring between July and September 2017

(SI Figure:S3). Due to low SS rates in the summer, there are no significant ‘peak events’ present in these series, and no clear delay relationships between the different locations during this summer period, suggesting strong SS peak signals are required for this analysis.

4 | DISCUSSION

4.1 | General discussion

Using the calibrations between SS and turbidity, along with discharge volumes, catchment erosion yields were calculated for the upstream catchment areas above Fosse Bridge and Bibury. Estimated catchment yields for these parts of the Coln catchment are typical of chalk and limestone catchments in the UK, which are generally the lowest recorded in the UK with sediment yields generally $\sim 10 \text{ t km}^{-2} \text{ year}^{-1}$ (Walling & Amos, 1999; Heywood & Walling, 2003). For the Coln, estimated sediment yields were generally $< 4 \text{ t km}^{-2} \text{ year}^{-1}$. It was found that estimates of the yearly SS exported from the catchment beyond Bibury were not dissimilar to those generated before Fosse Bridge, suggesting that on an annual basis, only relatively small increases in SS export occurred between Fosse Bridge and Bibury, except in 2018 (Table 2). This was the year when the equipment installation at Fosse bridge suffered from a lack of battery power in the early part of the year and was unable to effectively record discharge, for much of the monitoring period. Monthly analysis of

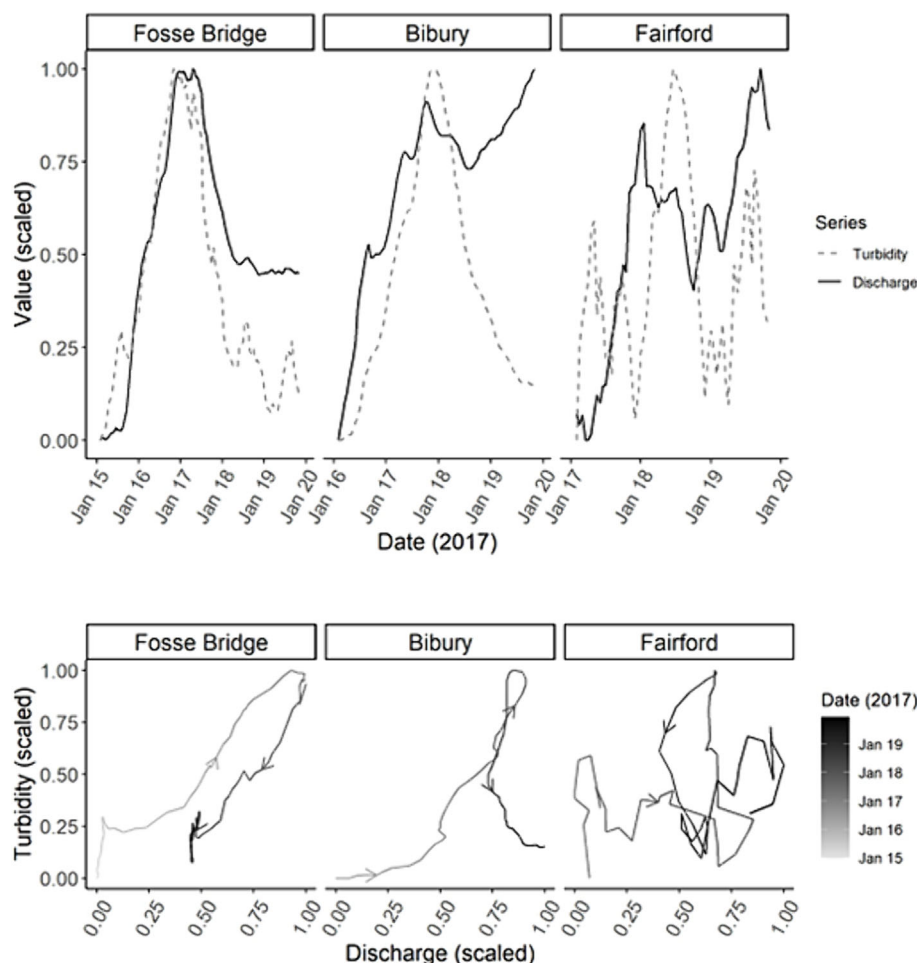


FIGURE 12 Diagram showing scaled (a) discharge and turbidity plots and (b) hysteresis plots for period 15th to 20th January 2017. [Color figure can be viewed at wileyonlinelibrary.com]

sediment export data demonstrated that the river between Fosse Bridge and Bibury occasionally acted as a short-term sediment sink when groundwater levels were low.

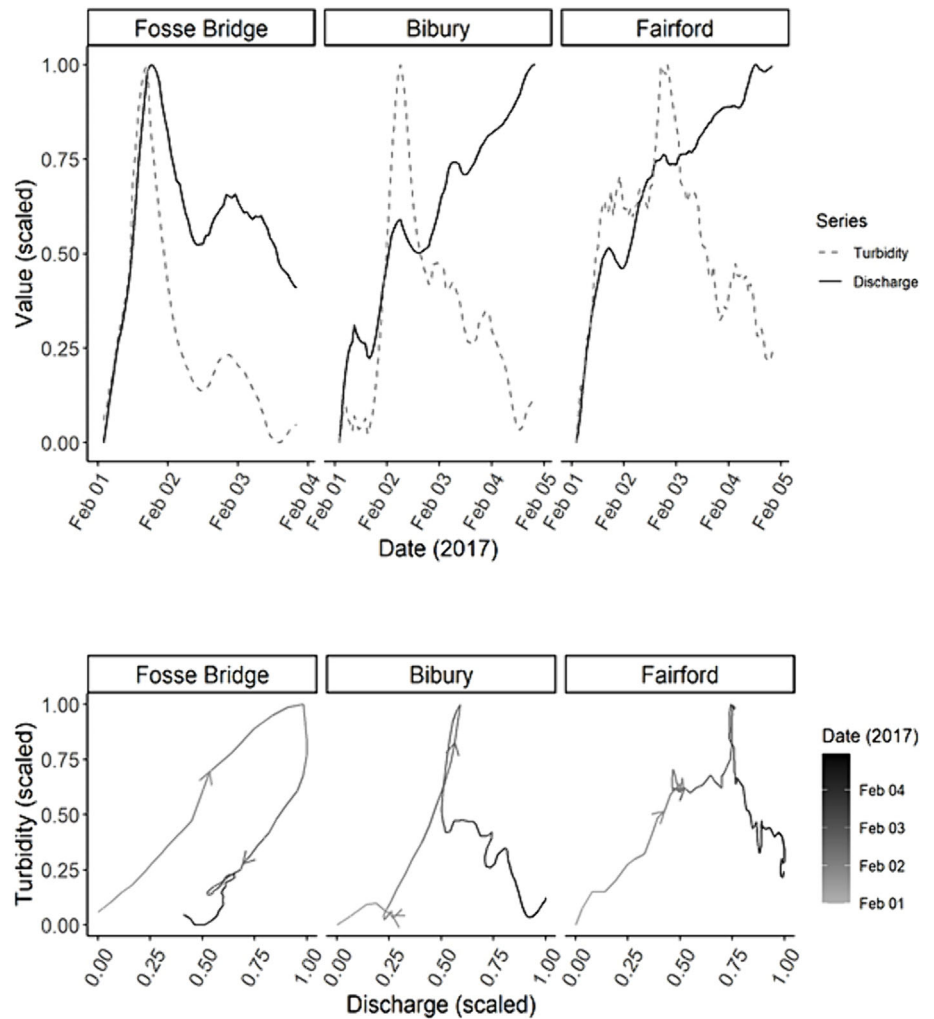
For a catchment with BFI > 0.9, sediment yield showed a strong seasonal response in turbidity and SS concentrations. Highest rates of sediment yield ($\text{t km}^2 \text{ year}^{-1}$) occurred during the winter, when the groundwater levels were highest, leading to increased water discharge. This was demonstrated by the relationship between monthly discharge and turbidity at Fosse Bridge and Bibury (Figure 5) and by the ARIMAX regression models (Section 3.5). However, turbidity events not connected to the overall base flow conditions were poorly modelled throughout the data series leading to high model residuals. Predicting turbidity is difficult, and many modelling approaches have been attempted (Gupta et al., 2021). It is the many, often random, erosion events that influence sediment generation, that are difficult to capture within the parameterisation of such models. In the current work, these may include (i) the assumption that the same relationships that drive turbidity apply throughout the year, (ii) the exact spatial and temporal pattern of rainfall across a portion of the catchment will influence turbidity (in a manner that is unknown to us) but at best can only be obtained from a limited number of rain gauge measurements, (iii) the turbidity time series includes some spikes which we do not have sufficient information to explain (e.g. bank collapse or erosion by cattle) and (iv) localised heavy rain storms or events. However, these models may be useful for specific purposes such as time series data gap filling where missing observations occur or the prediction of

future turbidity levels under different climate scenarios based upon expected discharge, groundwater and temperature values.

In relation to sediment source, key factors are that the Coln has a BFI > 0.9, no major tributaries and has buffer strips or grassland along its length. Thus, water velocity and discharge related to groundwater are likely to be major drivers increasing SS through its capacity to erode and entrain sediment from the riverbed and banks and suggests that they may be the major sources, particularly as erosion rates being $< 4 \text{ t km}^2 \text{ year}^{-1}$ suggests that other major sources of sediment are not present. However, other sediment sources such as road and tracks may be important as they offer a degree of connectivity in rural landscapes (Collins et al., 2012; Cooper et al., 2015; Boardman & Vandaele, 2023) or the role of grazing animals contributing to bank erosion. Insufficient sediment was collected in this study for source apportionment, but recent studies have shown their potential for determining sediment sources (Cooper et al., 2015).

Discharge and turbidity plots, hysteresis plots and wavelet analysis were undertaken on sections of the collected time series data. A general overview of sediment movement was obtained from these for the three sites. Overall, results described initial sediment flushing, followed by rapid drops in SS concentrations. These responses suggest that the system is largely sediment limited, and the limited surface hydrological connectivity and the use of buffer strips in the catchment suggest that turbidity was possibly linked more to bank and bed erosion than soil erosion. The overall trends found at the three sites can be summarised and each demonstrates different SS

FIGURE 13 Diagram showing scaled (a) discharge and turbidity plots and (b) hysteresis plots for period 1st to 5th February 2017. [Color figure can be viewed at wileyonlinelibrary.com]



transport dynamics at the monitoring stations. For Fosse Bridge, discharge and turbidity peaks were found to occur at similar times and accompanied by either clockwise or linear hysteresis plots. These suggest that sediment is initially available but becomes rapidly exhausted (Malutta et al., 2020). At Bibury, there was a tendency for anti-clockwise hysteresis plots to be found where the storm peak is ahead of the sediment wave. This is likely due to increases in base flow as the upstream catchment area increases and groundwater level rises. The anti-clockwise hysteresis response may also suggest that some sediment replenishment is occurring, possibly through bank erosion or transport of sediment from upstream (Malutta et al., 2020). At Fairford, anticlockwise hysteresis and rapid increases in SS are found, followed by sharp decreases in turbidity as storm discharge increases, suggesting that dilution effects occur as inputs from base flow increase. Thus, the data reveals three broad categories of sediment movement within the Coln catchment. A flushing of sediment prior to the Fosse Bridge monitoring station with the source likely being upstream in the headwaters, where the slopes are steepest. Secondly, at Bibury, an increase in water volume via base flow occurs, with some evidence of initial resuspension followed by transport of sediment from upstream on occasions, followed by sudden falls in sediment supply on other occasions, possibly caused by dilution. Thirdly, at Fairford, sediment peaks are slightly delayed compared to the storm wave with sediment supply becoming diluted.

As previously described, seasonal patterns of SS transport appeared to be present, with high turbidity events during winter or high discharge events being suitable for tracing groups of peaks downstream using wavelet analysis. However, this analysis was not possible in the section of time series data examined for the summer period (Jul–Oct 2017) due to low river discharge and SS concentrations. Whereas times of peak sediment concentrations at each of the monitoring stations during the explored events can be seen from the turbidity-discharge plots, wavelet analysis provides complementary information relating to estimates of the travel times of SS transport. The wavelet analysis demonstrates that patterns of SS generated upstream of Fosse Bridge can be traced down the river and that the SS peak group signal is not lost through deposition or through sediment dilution in the lower catchment. One reason is that the method focuses on the major peaks over a relatively long period of time. Travel times of SS were found to be approximately 16–18 h between Fosse Bridge and Bibury (10.5 km) and 19–25 h between Fosse Bridge and Fairford (22.9 km).

Results from the wavelet analysis suggest that sediment peaks mobilised in the upper catchment are identified, although diluted by groundwater inputs, particularly at Fairford, suggesting it may leave the catchment and enter the River Thames (Figure 1). Limestone streams are ecologically sensitive and support a wide range of biodiversity which may be impacted by SS. Developing better

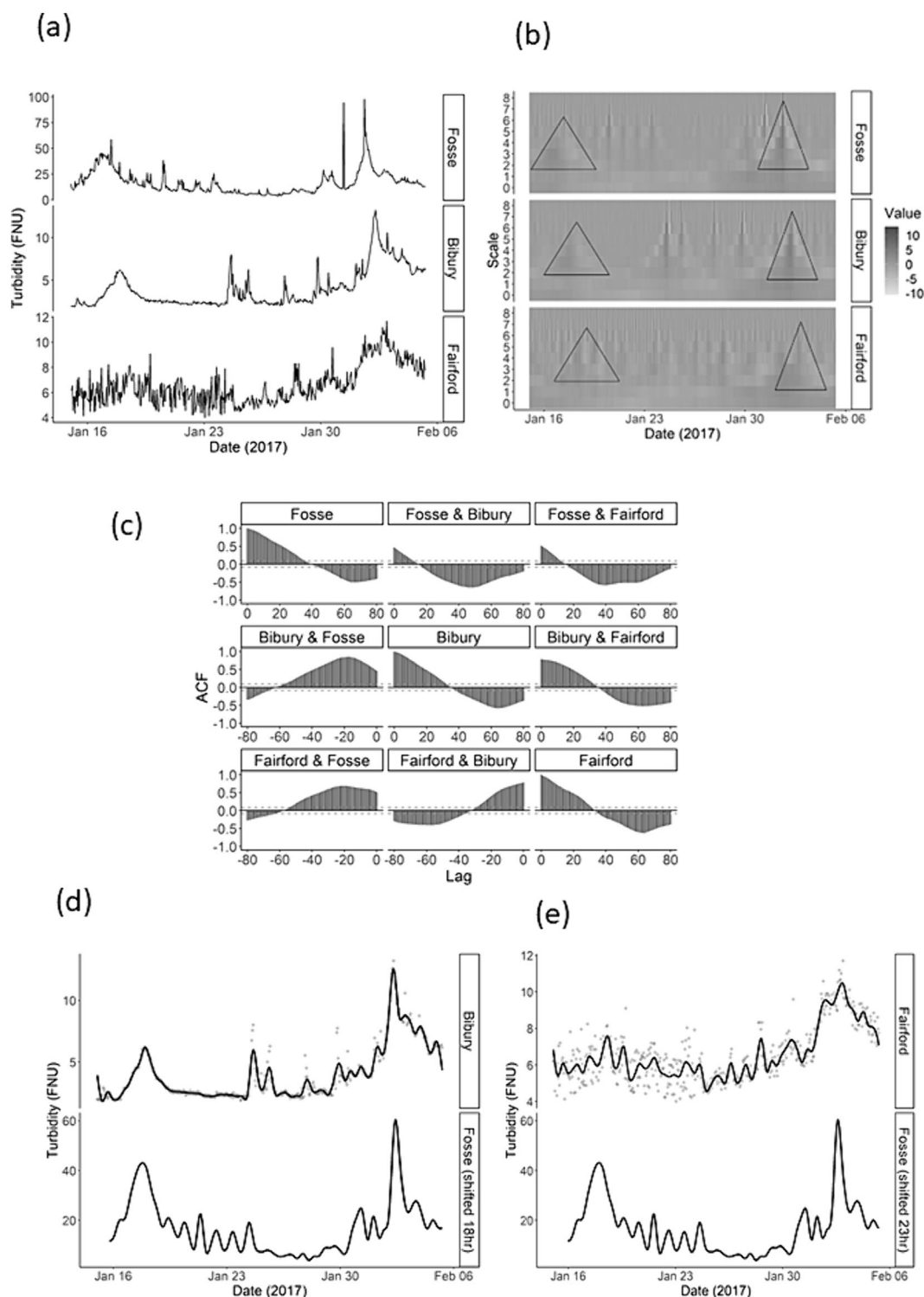


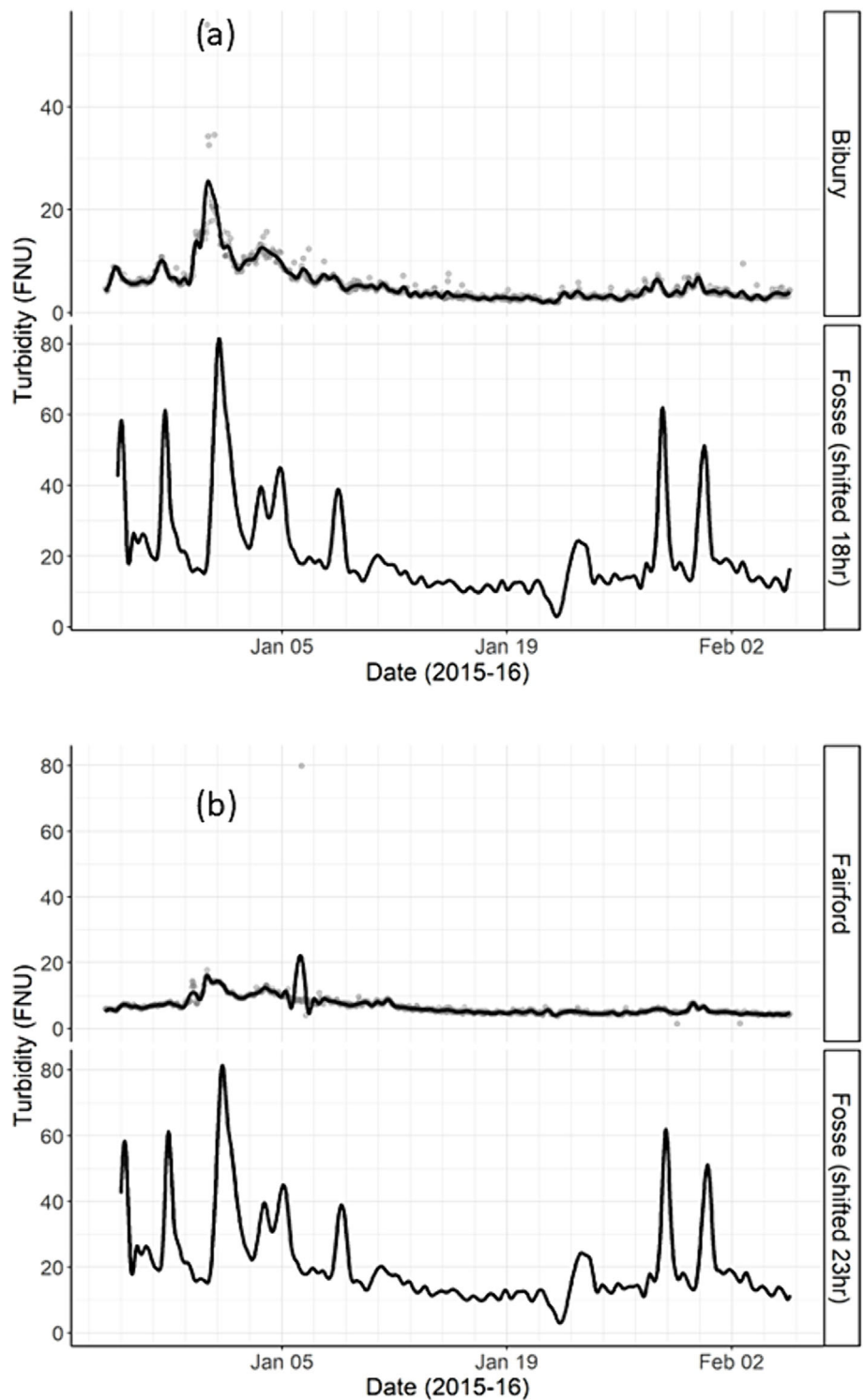
FIGURE 14 Figure showing (a) turbidity (FNU) time series for the time-period Jan–Feb 2017; (b) non-decimated wavelet transform coefficients of the turbidity time series from Fosse bridge, Bibury, and Fairford; (c) the estimated auto-correlation functions (ACF) for scale; and (d) delayed and scaled Fosse bridge smoothed series (black line) and firstly, Bibury and (e) secondly, Fairford (original points in grey and smoothed series black line). FNU, formazin nephelometric units.

understanding of the movement of SS is key to understanding some pressures these ecosystems face. The wavelet approach adds another layer of information regarding sediment dynamics including (i) how long sediment may remain suspended and (ii) how far it may travel. The period of sediment suspension is important as it demonstrates how long turbidity may impact (i) light levels, (ii) act as an irritant to for fish and other biota and (iii) help understand transport dynamics of sediment associated contaminants (e.g. P) including transport distance

and sorption/desorption (Geng et al., 2021; Jarvie et al., 2005; Vilman et al., 2015).

Whilst we tested the ‘wavelet’ approach in the Coln, which is a very simple river, the key would be to assess its suitability in more complicated river systems. The wavelet analysis was likely aided by the lack of tributaries entering the main river channel with associated influxes of sediment. This latter point reflects a key requirement in the development of extended turbidity sensor networks within a

FIGURE 15 Wavelet smoothed series of turbidity peaks delayed between Fosse bridge and (a) Bibury and (b) Fairford. [Color figure can be viewed at wileyonlinelibrary.com]



single river system. Careful consideration of placement, the number of sensors and statistical techniques is required to try and understand the complexity of SS dynamics.

4.2 | Potential limitations of the study

Whilst sensor networks enable the generation of high-resolution proxy datasets of SSC, potential sources of error need to be recognised. Many of these are well documented and include differences in FNU measurements between makes of turbidity sensors (e.g. due to different technologies, positioning of the sensor within

the instrument) and even between sensors of the same type. Methods of calibration (e.g. in-house according to manufacturer's instructions or in-situ) are also contested as to the best scenario (Tymaszewicz et al., 2017). Beyond the technology challenges, factors related to different river systems, and the impact of different sediment mineral assemblages and suspended particulate matter sources in the water column are recognised (Tymaszewicz et al., 2017). Thus, it is recommended that the reporting of turbidity as FNU for environmental standards or regulation should not be used. Instead FNU turbidity should be calibrated to the property that is of interest, such as SSC (Davies-Colley et al., 2021). In this study, individual calibration relationships between FNU turbidity and SSC were generated for Fosse

Bridge and Bibury. These relationships were found to be reasonably similar, based on the calibration methods and maintenance of the network undertaken by NWQIS. As the Coln has no real tributaries, this may also limit the number of different mineralogical sources, helping to produce the similar calibrations. However, whilst it is good practice to use individual calibration curves, results of a single calibration ($SS = 0.00105 * \text{Turbidity} + 0.00042$, with an R^2 of 0.96) combining results from Fosse Bridge and Bibury were generated (SI Table S4). These outputs can be compared to those in Table 4. For Fosse Bridge, results from both calibrations were reasonably close and this may reflect the greater range of turbidity values at this site, and influence within the combined calibration. At Bibury, results using the combined calibration were 35%–40% lower for SS export and yield. These results demonstrate the need for individual calibrations. However, for other aspects of the study, FNU are used as the interest is in monitoring the change in turbidity over time and this is best undertaken on the FNU data as converting to SSC will introduce error, especially in a system with low SSC. Whilst this study has SSC of $< 0.2 \text{ g L}^{-1}$, many studies deal with much greater SSC concentration (e.g. Stutter et al., 2017; Uhrich & Bragg, 2003).

When designing automated sampling systems, there are trade-offs associated with the practicalities of physically installing systems (e.g. width and depth of channel), cost (e.g. maintenance) and in relation to the purpose and use of the data. Whilst some authors (e.g. Davies-Colley et al., 2021) prefer in-situ calibration, this again depends on the circumstance. The instruments set up in the current work were calibrated and maintained according to the protocols developed for operating a national sensor network. This requires a consistency of approach, along with cost and efficiency issues. Therefore, laboratory calibration according to the manufacturers recommendations was undertaken (Exo-user manual). However, by using NWQIS to maintain the experimental set up and by using the same model of sensor at the three sites, major attempts to minimise errors associated with sensors were taken.

Potential issues relating to depth sampling through the river profile need also to be considered. In this study, a single inlet for water was used. Previous studies have suggested that this approach may lead to under-estimation of turbidity measurements in rivers with high sand concentrations as samples are not withdrawn isokinetically (USGS, 2006). This latter approach potentially allows greater accuracy through better representation of suspended sand sized particles close to the riverbed. However, Gray & Landers (2014) suggest that at low velocity ($< 0.6 \text{ m s}^{-1}$) little or no sand is transported. Fosse Bridge is the fastest part of the catchment and typically velocity remained below 0.6 m s^{-1} . Only very occasionally in the wet winter of 2015–2016 did daily average velocity exceed 0.6 m s^{-1} (see SI: Figure S5), suggesting that export and yield estimates are likely not to have produced large underestimates in sand transport for the majority of the time series. As described in Section 2.2, efforts were made in the design phase to tailor a system to the previously known physical attributes of the Coln, which is low velocity, shallow at sampling points and has the potential for low flows in the upper catchment. At Fosse Bridge, the average annual water depth was $\sim 40 \text{ cm}$. At Bibury, an average annual water depth of $\sim 25 \text{ cm}$ was recorded. Thus, the design was considered to provide as representative a sample as possible, with potential sources of error minimised. Depth dependent sampling using isokinetic samplers within the Coln would be difficult

as the river velocity was often below or at the limits of recommended flow rates for samplers. The average velocity at Fosse Bridge, the steepest part of the catchment, over the sampling period was 0.27 m s^{-1} . Requirements for isokinetic samplers (USGS, 2006) have been suggested to be between 1.5 and 3 ft s^{-1} ($0.45\text{--}0.90 \text{ m s}^{-1}$).

5 | CONCLUSIONS

SS dynamics were investigated in the River Coln. The catchment exhibited low SS yields, with values typically in the range for UK limestone or chalk-based systems with high base flow. Hysteresis analysis showed the river system was largely sediment limited with rapid export of available sediment. This reflects low soil erosion and surface hydraulic connectivity within the catchment, and the land-use protections used to limit soil erosion. The hysteresis analysis and the wavelet transforms demonstrate that even in a relatively simple river and sediment system such as the Coln, the dynamics of SS transport is complex, with different processes operating at different distances from the headwaters. However, the capability to creatively design and install turbidity sensor systems to examine SS transport through rivers systems and combining them with advanced time series statistical analysis offers new opportunities to understand SS transport (Droujko et al., 2023) and monitor the impact of changing land management practices. This could be facilitated by the design and manufacture of low-cost turbidity sensors (Droujko & Molnar (2022)). The results provide further evidence that wavelet transforms can be used to describe SS events (Gupta et al., 2021). Increasingly, high-resolution datasets of turbidity measurements are being analysed using artificial intelligence (AI) techniques, particularly to identify the number and types of hysteresis events that occur (Gupta et al., 2021). These AI techniques open further possibilities for exploring large high-resolution datasets such as the one described in this paper, to generate greater understanding on sediment transport dynamics in ecologically sensitive river systems.

ACKNOWLEDGEMENTS

The project was a BGS National Capability research project (NEE71855) funded by Natural Environment Research Council (NERC). The authors would like to thank Prof. Mike Ellis for his contribution to developing the project and to Matt Loewenthal and Rik Smith at NWQIS for establishing and maintaining the sensor network. AT, BM, and KL publish with the permission of the Director of the British Geological Survey.

DATA AVAILABILITY STATEMENT

Data is available from the corresponding author on request.

ORCID

Andrew M. Tye  <https://orcid.org/0000-0002-4653-7773>

REFERENCES

- Acornley, R.M. & Sear, D.A. (1999) Sediment transport and siltation of brown trout (*Salmo trutta* L.) spawning gravels in chalk streams. *Hydrological Processes*, 13(3), 447–458. Available from: [https://doi.org/10.1002/\(SICI\)1099-1085\(19990228\)13:3<447::AID-HYP749>3.0.CO;2-G](https://doi.org/10.1002/(SICI)1099-1085(19990228)13:3<447::AID-HYP749>3.0.CO;2-G)

- Asselman, N.E.M. (2000) Fitting and interpretation of sediment rating curves. *Journal of Hydrology*, 234(3-4), 228–248. Available from: [https://doi.org/10.1016/S0022-1694\(00\)00253-5](https://doi.org/10.1016/S0022-1694(00)00253-5)
- Boardman, J. & Vandaele, K. (2023) Soil erosion and runoff: the need to rethink mitigation strategies for sustainable agricultural landscapes in western Europe. *Soil Use and Management*, 39(2), 673–685. Available from: <https://doi.org/10.1111/sum.12898>
- Boardman, J., Vandaele, K., Evans, R. & Foster, I.D.L. (2019) Off-site impacts of soil erosion and runoff: why connectivity is more important than erosion rates. *Soil Use and Management*, 35(2), 245–256. Available from: <https://doi.org/10.1111/sum.12496>
- Bowes, M.J., Armstrong, L.K., Harman, S.A., Wickham, H.D., Nicholls, D.J.E., Scarlett, P.M., et al. (2018) Weekly water quality monitoring data for the river Thames (UK) and its major tributaries (2009–2013): the Thames initiative research platform. *Earth System Science Data*, 10(3), 1637–1653. Available from: <https://doi.org/10.5194/essd-10-1637-2018>
- Collins, A.L. & Anthony, S.G. (2008) Assessing the likelihood of catchments across England and Wales meeting 'good ecological status' due to sediment contributions from agricultural sources. *Environmental Science & Policy*, 11(2), 163–170. Available from: <https://doi.org/10.1016/j.envsci.2007.07.008>
- Collins, A.L., Walling, D.E., Webb, L. & King, P. (2010) Apportioning catchment scale sediment sources using a modified composite fingerprinting technique incorporating property weightings and prior information. *Geoderma*, 155(3), 249–261. Available from: <https://doi.org/10.1016/j.geoderma.2009.12.008>
- Collins, A.L., Zhang, Y., McChesney, D., Walling, D.E., Haley, S.M. & Smith, P. (2012) Sediment source tracing in a lowland agricultural catchment in southern England using a modified procedure combining statistical analysis and numerical modelling. *Science of The Total Environment*, 414, 301–317. Available from: <https://doi.org/10.1016/j.scitotenv.2011.10.062>
- Cooper, R.J., Krueger, T., Hiscock, K.M. & Rawlins, B.G. (2015) High-temporal resolution fluvial sediment source fingerprinting with uncertainty: a Bayesian approach. *Earth Surface Processes and Landforms*, 40(1), 78–92. Available from: <https://doi.org/10.1002/esp.3621>
- Davies-Colley, R., Hughes, A.O., Vincent, A.G. & Heubeck, S. (2021) Weak numerical comparability of ISO-7027-compliant nephelometers. Ramifications for turbidity measurement applications. *Hydrological Processes*, 35(12), e14399.
- Droujko, J. & Molnar, P. (2022) Open-source, low cost, in-situ turbidity sensor for river network monitoring. *Scientific Reports*, 12(1), 10341. Available from: <https://doi.org/10.1038/s41598-022-14228-4>
- Droujko, J., Sudha, S.H., Singer, G. & Molnar, P. (2023) Sediment source and sink identification using Sentinel-2 and a small network of turbidimeters on the Vjosa River. *Earth Surface Dynamics*, 11, 881–897.
- Environment Agency website. a guidance-document-containing-further-details-and-drawings-to-help-with-your-volume-estimates.pdf (environment-agency.gov.uk); accessed Jan 24
- EXO User Manual. — advanced water quality monitoring platform user manual item 603789. <exo-user-manual-web.pdf> (ysi.com)
- Ferreira, C.S.S., Walsh, R.P.D. & Ferreira, A.J.D. (2018) Degradation in urban areas. *Current Opinion in Environmental Science & Health*, 5, 19–25. Available from: <https://doi.org/10.1016/j.coesh.2018.04.001>
- Findlay, D.C., Colborne, G.J.N., Cope, D.W., Harrod, T.R., Hogan, D.V. & Staines, S.J. (1984) Soils and their use in south-West England. *Soil Survey of England and Wales Bulletin*, 14, 230–232.
- Fryirs, K.A. (2013) (Dis)connectivity in catchment sediment cascades: a fresh look at the sediment delivery problem. *Earth Surf Process Landforms*, 38, 30–46. Available from: <https://doi.org/10.1002/esp.3242>
- Geng, X., Li, D., Xu, C. & Sun, P. (2021) Using sediment resuspension to immobilize sedimentary phosphorus. *Environmental Science and Pollution Research*, 28(2), 1837–1849. Available from: <https://doi.org/10.1007/s11356-020-10602-9>
- Gray, J.R. & Landers, M.N. (2014) Measuring suspended sediment. In: Ahuja, S. (Ed.) *Comprehensive water quality and purification*, Vol. 1. United States of America: Elsevier, pp. 157–204 <https://doi.org/10.1016/B978-0-12-382182-9.00012-8>
- Gupta, D., Hazarika, B.B., Berlin, M., Sharma, U.M. & Mishra, K. (2021) Artificial intelligence for suspended sediment load prediction: a review. *Environmental Earth Sciences*, 80(9), 346. Available from: <https://doi.org/10.1007/s12665-021-09625-3>
- Haddadchi, A. & Hicks, M. (2021) Interpreting event based suspended sediment concentration and flow hysteresis patterns. *Journal of Soils and Sediments*, 21(1), 592–612. Available from: <https://doi.org/10.1007/s11368-020-02777-y>
- Heywood, M.J.T. & Walling, D.E. (2003) Suspended sediment fluxes in chalk streams in the Hampshire catchment, U.K. *Hydrobiologia*, 494, 111–117.
- Hodge, C.A.H., Burton, R.G.O., Corbett, W.M., Evan, R. & Seale, R.S. (1984) Soils and their use in eastern England. *Soil Survey of England and Wales Bulletin*, 13, 310–312.
- Jarvie, H.P., Jürgens, M.D., Williams, R.J., Neal, C., Davies, J.J.L., Barrett, C., et al. (2005) Role of river bed sediments as sources and sinks of phosphorus across two major eutrophic UK river basins: the Hampshire Avon and Herefordshire wye. *Journal of Hydrology*, 304(1-4), 51–74. Available from: <https://doi.org/10.1016/j.jhydrol.2004.10.002>
- Littlewood, I.G., Watts, C.D. & Custance, J.M. (1998) Systematic application of United Kingdom river flow and quality databases for estimating annual river mass loads. *Science of the Total Environment*, 210(211), 21–40. Available from: [https://doi.org/10.1016/S0048-9697\(98\)00042-4](https://doi.org/10.1016/S0048-9697(98)00042-4)
- Mackey, A.P., Ham, S.F., Cooling, D.A., & Berrie, A.D. (1982) An ecological survey of a limestone stream, the River Coln, Gloucestershire, England, in comparison with some other chalk streams. *Archiv f. Hydrobiologie, Suppl.-Bd.64*.
- Malutta, S., Kobiyama, M., Chaffe, P.L.B. & Bernardi Bonumá, N. (2020) Hysteresis analysis to quantify and qualify the sediment dynamics: state of the art. *Water Science and Technology*, 81(12), 2471–2487. Available from: <https://doi.org/10.2166/wst.2020.279>
- Met Office. 2019. UKCP18 science overview executive summary January 2019. Crown Copyright 2019
- Nason, G.P. (2016) wavethresh: wavelets statistics and transforms. R package version 4.6.8 NRFA. <https://nrfa.ceh.ac.uk>; accessed Jan 2024
- Nason, G.P. & Silverman, B.W. (1995) *The stationary wavelet transform and some statistical applications in wavelets and statistics*. New York, NY: Springer Verlag, pp. 281–299.
- Parra, L., Ahmad, A., Sendra, S., Lloret, J. & Lorenz, P. (2024) Combination of machine learning and RGB sensors to quantify and classify water turbidity. *Chem*, 12(3), 34. Available from: <https://doi.org/10.3390/chemosensors12030034>
- Rasmussen, P.P., Gray, J.R., Glysson, G.D., and Ziegler, A.C., 2009, Guidelines and procedures for computing time-series suspended-sediment concentrations and loads from in-stream turbidity-sensor and streamflow data: U.S. Geological Survey Techniques and Methods, book 3, chap. C4, 52 p.
- Rymaszewicz, A., O'Sullivan, J.J., Bruen, M., Turner, J.N., Lawler, D.M., Conroy, E., et al. (2017) Measurement differences between turbidity instruments, and their implications for suspended sediment concentration and load calculations: a sensor inter-comparison study. *Journal of Environmental Management*, 199, 99–108. Available from: <https://doi.org/10.1016/j.jenvman.2017.05.017>
- Stott, T., Leeks, G., Marks, S. & Sawyer, A. (2001) Environmentally sensitive plot-scale timber harvesting: impacts on suspended sediment, bedload and bank erosion dynamics. *Journal of Environmental Management*, 63(1), 3–25. Available from: <https://doi.org/10.1006/jema.2001.0459>
- Stott, T.A. (2020) Do riparian buffer zones and new forest management practices reduce stream suspended sediment loads?: re-visiting the Afon Tanllwyth in Hafren Forest, Plynlimon, 20 years on. *Soil Use and Management*, 37(4), 921–935. Available from: <https://doi.org/10.1111/sum.12670>
- Stutter, M., Dawson, J.J.C., Glendell, M., Napier, F., Potts, J.M., Sample, J., et al. (2017) Evaluating the use of in-situ turbidity meters to quantify

- sediment and phosphorus concentrations and fluxes in agricultural streams. *Science of the Total Environment*, 607-608, 391-402. Available from: <https://doi.org/10.1016/j.scitotenv.2017.07.013>
- Thollet, F., Rousseau, C., Camenen, B., Boubkraoui, S., Branger, F., Lauters, F., et al. (2021) Long term high frequency sediment observatory in an alpine catchment: the arc-Isère rivers, France. *Hydrological Processes*, 35, e14044. Available from: <https://doi.org/10.1002/hyp.14044>
- Uhrich, M.A., Bragg, H.M. (2003) Monitoring instream turbidity to estimate continuous suspended-sediment loads and yields in the Upper North Santiam River Basin, Oregon, 1998-2000. U.S. Geological Survey Water Resources Investigations Report 03-4098, 43pp.
- USGS. (2006) National field manual for the collection of water-quality data: chapter 4A. Collection of water samples. In Book 9: Handbooks for Water-Resources Investigations.
- Vercruyse, K., Grabowski, R.C., Hess, T. & Lexartza-Areza, I. (2020) Linking temporal scales of suspended sediment transport in rivers: towards improving transferability of prediction. *Journal of Soils and Sediments*, 20(12), 4144-4159. Available from: <https://doi.org/10.1007/s11368-020-02673-5>
- Vercruyse, K., Grabowski, R.C. & Rickson, R.J. (2017) Suspended sediment transport dynamics in rivers: multi-scale drivers of temporal variation. *Earth-Science Reviews*, 166, 38-52. Available from: <https://doi.org/10.1016/j.earscirev.2016.12.016>
- Vilman, L., Aissa-Grouz, N., Garnier, J., Billen, G., Mouchel, J.-M., Poulin, M., et al. (2015) Impacts of hydro-sedimentary processes on the dynamics of soluble reactive phosphorus in the Seine river. *Biogeochemistry*, 122(2-3), 229-251. Available from: <https://doi.org/10.1007/s10533-014-0038-3>
- Walling, D.E. (1977) Assessing the accuracy of suspended sediment rating curves for a small basin. *Water Resources Research*, 13(3), 531-538. Available from: <https://doi.org/10.1029/WR013i003p00531>
- Walling, D.E. & Amos, C.M. (1999) Source, storage and mobilisation of fine sediment in a chalk stream system. *Hydrological Processes*, 13(3), 323-340. Available from: [https://doi.org/10.1002/\(SICI\)1099-1085\(19990228\)13:3<323::AID-HYP741>3.0.CO;2-K](https://doi.org/10.1002/(SICI)1099-1085(19990228)13:3<323::AID-HYP741>3.0.CO;2-K)
- Worrall, F., Howden, N.J.K. & Burt, T.P. (2013) Assessment of sample frequency bias and precision in fluvial flux calculations – an improved low bias estimation method. *Journal of Hydrology*, 503, 101-110. Available from: <https://doi.org/10.1016/j.jhydrol.2013.08.048>

SUPPORTING INFORMATION

Additional supporting information can be found online in the Supporting Information section at the end of this article.

How to cite this article: Tye, A.M., Leeming, K.A., Gong, M., Marchant, B. & Hurst, M.D. (2024) Assessment of suspended sediment export and dynamics using in-line turbidity sensors and time series statistical models. *Earth Surface Processes and Landforms*, 49(13), 4113-4132. Available from: <https://doi.org/10.1002/esp.5952>